Ab initio equation of state data for hydrogen, helium, and water and the internal structure of Jupiter

Nadine Nettelmann, Bastian Holst, André Kietzmann, Martin French, and Ronald Redmer

Institut für Physik, Universität Rostock, D-18051 Rostock, Germany

nadine.nettelmann@uni-rostock.de

David Blaschke

Institute for Theoretical Physics, University of Wroclaw, Max-Born pl. 9, 50-204 Wroclaw, Poland

ABSTRACT

The equation of state of hydrogen, helium, and water effects interior structure models of giant planets significantly. We present a new equation of state data table, LM-REOS, generated by large scale quantum molecular dynamics simulations for hydrogen, helium, and water in the warm dense matter regime, i.e. for megabar pressures and temperatures of several thousand Kelvin, and by advanced chemical methods in the complementary regions. The influence of LM-REOS on the structure of Jupiter is investigated and compared with state-of-the-art results within a standard three-layer model consistent with astrophysical observations of Jupiter. Our new Jupiter models predict an important impact of mixing effects of helium in hydrogen with respect to an altered compressibility and immiscibility.

Subject headings: planets and satellites: individual (Jupiter) – equation of state

1. Introduction

Jupiter consists by more than 85% in mass of hydrogen and helium. Among the minor constituents, oxygen contributes the largest fraction. Although the major constituents are rather simple elements, they occur almost exclusively in extreme, up to now largely unknown states of matter. For instance, about 90% of the planetary material in Jupiter is in a high-pressure state beyond the 1 Mbar level up to about 70 Mbar in the center, and the temperature varies by two orders of magnitude from the cold and dilute outer envelope up to about 20.000 K in the deep interior. In terms of usual plasma parameters, the interior

covers the transition from weak to strong ion coupling, and from weak to moderate electron degeneracy without relativistic effects. Giant planets like Jupiter are therefore particularly suitable to study *warm dense matter* (WDM), especially mixtures of H, He, and H_2O.

In this paper we apply for the first time ab initio equation of state (EOS) data for H, He, and H_2O, representing at least 97% of the planetary material in Jupiter, to interior models in order to derive more reliable implications for an improved structure model as well as for the H/He phase diagram. We have performed large scale quantum molecular dynamics simulations for the WDM region and applied advanced chemical models in the complementary regions. These EOS data for the major components were combined by linear mixing into a new data table LM-REOS (Linear Mixing Rostock Equation of State). Fundamental problems concerning hydrogen and helium such as the location of the nonmetal-to-metal transition (NMT), whether or not this transition is accompanied by a thermodynamic phase instability - the plasma phase transition (PPT) -, and the existence of a miscibility gap are at the same time key issues for the construction of planetary models.

Strongly improved high-pressure data for planetary materials as well as new and more accurate observational data for Jupiter and the other planets have motivated intensive efforts to model giant planets. We outline briefly major steps in the development of planetary models that lead to our present understanding of Jupiter's interior structure.

In one of the first approaches, Hubbard (1968) started from estimates of Jupiter's net heat flux and inferred a slightly superadiabatic temperature gradient, causing convective instability throughout the planet. With his fully homogeneous and, thus, overdetermined model he compared with current observational constraints in order to discriminate between different equations of state (Hubbard 1969).

Stevenson & Salpeter (1977a,b) examined the transport properties of hydrogen-helium mixtures and the influence of a PPT and of H/He phase separation on the structure and evolution of hydrogen-helium planets. Either of these processes would divide the fluid interior into two convective layers, a molecular outer envolope and a metallic inner envelope with different helium abundances. The NMT was predicted to occur around 2-4 Mbar, and helium immiscibility between 4-40 Mbar and below 8000 K. Depending on the true position of the NMT coexistence line and the demixing curve in the H/He phase diagram, the extension of the inhomogeneous, diffusive transition region in between could be very narrow. Minor constituents were argued to be redistributed in consequence of helium immiscibility.

Voyager data indeed unveiled a depletion of helium in the outer molecular envelope, indicating that H/He phase separation has happened there. A thermodynamically consistent H-EOS was developed by Saumon & Chabrier (1992) for astrophysical applications within a

chemical model that predicted a discontinuous NMT. This PPT has been proposed for a long time (Norman & Starostin 1968, 1970; Zeldovich & Landau 1944) and the phase diagram was discussed in detail (Beule et al. 2001; Ebeling & Norman 2003; Holst et al. 2007). A first experimental signature for a PPT in deuterium was given quite recently (Fortov et al. 2007). Using this H-EOS, the observational constraints for Jupiter could only be adjusted if the envelopes were allowed to have a density discontinuity, and if a several Earth masses sized core of rocks and ices was admitted (Chabrier et al. 1992). For simplicity, helium was (and in recent models still is) added to the EOS of hydrogen via the additive volume rule, and the fraction of helium in both envelopes was used to adjust the gravitational moments J_2 and J_4. Other constituents than hydrogen and helium - summarized as heavy elements or metals - were represented by helium too.

A significant step forward in constructing reliable Jupiter models was done by Guillot (1999a,b) who used an improved computer code (Guillot & Morel 1995), improved EOS data of Saumon, Chabrier & Van Horn (1995) (SCvH), and more accurate observational data for the atmospheric helium abundance from the Galileo mission (von Zahn et al. 1998). This improved Jupiter model predicted a core mass of 0-10 Earth masses ($M_\oplus$), a total amount of heavy elements of 11-41 $M_\oplus$, and a heavy element enrichment of up to 6.5 times the solar value in the molecular region. The great margins resulted from a variation of the observables within their error bars, but most of all from the uncertainty in the H-EOS data itself in the region around the NMT. By choosing appropriate pair potentials for the H_2 molecules, the underlying H-EOS (H-SCvH-ppt) was constructed to reproduce shock compression data derived from gas gun experiments (Nellis et al. 1983; Thiel et al. 1973). A first-order phase transition was found around 2 Mbar, the slightly decreasing coexistence line ends in a second critical point at about 15000 K. Its interpolated version (H-SCvH-i) has been widely used in planetary modelling (Gudkova & Zharkov 1999; Guillot 1999a; Saumon & Guillot 2004). As before (Chabrier et al. 1992), the fraction of metals was obtained from the excess density with respect to that of a given H/He mixture.

In an alternative approach, Kerley (2004a) calculated three-layer models (a core of rocks or ices and two fluid envelopes) using a revised Sesame EOS for H (Kerley 2003), an improved He-EOS (Kerley 2004b), and the PANDA code for the icy components H_2O, NH_3, CH_4, and H_2S and their atomic constituents to represent metals. Choosing threefold enrichment in heavy elements in accordance with measurements (Atreya et al. 2003; Mahaffy 2000) for the molecular envelope, an enrichment of 7.5 times solar was required in the metallic envelope to match J_2, in total 35 $M_\oplus$. The large heavy element enrichment in the inner envelope was argued to result from a dispersion of planetesimals during the formation process.

The latest extensive calculations of Jupiter models have been performed (Saumon & Guillot

2004) using the Sesame EOS 7154 of water and the Sesame EOS 7100 of dry sand to represent metals within the envelopes and for hydrogen using the simple linear mixing (LM) model of Ross (Holmes et al. 1995). The LM model served as a basis for the generation of different H-EOS representing the current uncertainty on the experimental deuterium EOS data. Not all of the H-EOS applied gave satisfactory results. While acceptable Jupiter models were placed within the range of the previous models cited above, some LM-variants as well as the original Sesame EOS 5263 were not compatible with Jupiter's gravitational properties or age.

Other attempts (Holst et al. 2007) to construct Jupiter models with the Sesame EOS of hydrogen or a combination of fluid variational theory with plasma effects (FVT^+) (Holst et al. 2007) also failed to reproduce the observational constraints.

To decide whether a mismatch between calculated and observed parameters is due to an inaccuracy of the EOS or due to improper assumptions in the planetary model, accurate experimental data for the high-pressure phase diagram of hydrogen and hydrogen-helium mixtures are much-needed. Various experiments have been performed in the recent years to study the complex physical behavior of hydrogen in the region up to several Mbar (Boriskov et al. 2005; Collins et al. 1998; Knudson et al. 2004; Weir et al. 1996). The transition from a non-conducting, molecular fluid to an atomic, conducting fluid can be derived from electrical conductivity (Nellis et al. 1996) as well as reflectivity data (Celliers 2000). For instance, the NMT in fluid hydrogen at temperatures of about 3000 K has been pinpointed at 1.4 Mbar in multiple shock wave experiments (Weir et al. 1996). Reflectivity measurements indicate an NMT along the Hugoniot curve at about 0.5 Mbar (Celliers 2000). Most recently, the first experimental signature of a first-order phase transition connected with this NMT has been found in quasi-isentropic shock compression experiments in deuterium (Fortov et al. 2007). The maximum compression ratio along the principal Hugoniot curve of hydrogen is not ultimately fixed but a value of 4.25 has been found in various shock-wave experiments (Boriskov et al. 2005; Knudson et al. 2004) which is not predicted by any of the theoretical H-EOS mentioned above except the Sesame EOS.

On the other hand, current ab initio calculations yield not only agreement with experimental Hugoniot curves (Lenosky et al. 2000; Desjarlais 2003; Bonev et al. 2004; Holst et al. 2008) but also with reflectivity data (Collins et al. 2001; Mazevet et al. 2003; Holst et al. 2008) at high pressures. Therefore, we use in this study ab initio EOS data derived from extensive quantum molecular dynamics (QMD) simulations for the most abundant planetary materials hydrogen (Holst et al. 2008), helium (Kietzmann et al. 2007), and water (French et al. 2008) and study the impact of these data on models of Jupiter within the three-layer structure assumption.

Our paper is organized as follows. In the following section we describe our procedure to calculate three-layer planetary models. In §3 the new LM-REOS data tables for H, He, and H_2O are introduced and the differences to the widely used SCvH EOS are exemplified by means of the Jupiter isentrope and the relevant plasma parameters. Our results for Jupiter are presented in §4. First, our numerical results are checked by using the SCvH EOS. We then process the new LM-REOS data tables and compare the predictions for Jupiter's interior with previous results (Guillot 1999a; Guillot et al. 2003) and with additional calculations using the SCvH-ppt EOS regarding the distribution of chemical species. We discuss our results for Jupiter in §5 and propose key issues for future work on high-pressure EOS data and improvements of planetary models. A summary is given in §6.

2. Three-layer planetary models

2.1. Parameters for Jupiter

Our interior models follow the approach described in detail by Guillot (1999a). The planet is assumed to consist of three layers: two fluid, homogeneous, and isentropic envelopes composed of hydrogen, helium and metals and an isothermal core of rocks or ices.

For given EOS of these materials, the precise fractions of helium and metals within the envelopes and the size of the core are constrained by the requirement of matching the observational constraints, see Tab. 1. Jupiter's mass-radius relation (total mass $M_{\rm J}$, equatorial radius R_{eq}) requires the dominant mass fraction to be attributed to hydrogen (Guillot 2005). The mean helium fraction $\bar{Y}$ is assumed to reflect the hydrogen-helium ratio of the protosolar cloud. Due to the assumption of homogeneous layers the atmospheric helium fraction $Y_{\rm mol}$ is assigned to the whole outer envelope, starting at the 1 bar level with temperature T_1. The adjustment of the gravitational moments J_2 and J_4 assuming rigid rotation with angular velocity ω sets limits to the fraction of metals $Z_{\rm mol}$ in the outer envelope and $Z_{\rm met}$ in the inner envelope. Observational error bars translate into uncertainties of the resulting values of these structure properties, allowing for a variety of *acceptable* models. Comparing acceptable models with other predictions, such as from formation theory or abundance measurements, allows to evaluate the models, see §5.

Table 1. Measured data that are considered in the modelling procedure.

Parameter	Jupiter [a]
mass $M_{\rm J}$ [g]	$1.8986112(15) \times 10^{30}$
equatorial radius R_{eq} [m]	$7.1492(4) \times 10^{7}$ [b]
average helium mass fraction $\bar{Y}$	$0.275^{+0.003}_{-0.005}$ [c]
helium mass fraction $Y_{\rm mol}$	0.238(7) [d]
temperature T_1 [K]	165-170 [e]
angular velocity ω	$2\pi/9{\rm h}55$ [b]
$J_2/10^{-2}$	1.4697(1) [b]
$J_4/10^{-4}$	-5.84(5) [b]

[a]Numbers in parenthesis are the uncertainty in the last digits of the given value.

[b]taken from Guillot et al. (2003).

[c]Bahcall (1995).

[d]von Zahn et al. (1998).

[e]taken from Guillot (1999a)

Besides being the simplest interior structure model that is consistent with the observational constraints mentioned above, the three-layer stucture has been discussed and evaluated in connection with various underlying or neglected physical properties (Guillot 1999a). For instance, a small opacity could occur in a narrow region around 1500 K (Guillot et al. 1994a,b), causing a stable radiative layer and thus lengthen the cooling time of the planet without affecting the element distribution. Differential rotation is observed in the atmosphere and could modify J_2 up to 0.5% and J_4 up to 1% (Zharkov & Trubitsyn 1978). Assuming more than two envelopes would probably reflect the real structure of Jupiter more adequately, but also entail more degrees of freedom than can be adjusted by the constraints presently available.

Layer boundaries that devide the fluid planet into convective layers with different compositions have been predicted theoretically from general thermodynamic properties of warm dense hydrogen and hydrogen-helium mixtures (Stevenson & Salpeter 1977a,b). Possible sources of inhomogeneity from thermodynamic considerations are phase separation due to first-order phase transitions or immiscibility between different components, and from evolution theory the presence of a slowly eroding core. In case of Jupiter, the PPT in hydrogen is a candidate for an important first-order phase transition, besides those for the minor constituents as, e.g., H_2O in the outermost shells. Phase separation may occur between neutral helium and metallic hydrogen near the PPT of hydrogen (Klepeis et al. 1991; Pfaffenzeller et al. 1995). Both effects motivate a three-layer structure assumption.

2.2. Basic equations

The construction of acceptable interior models is performed in an iterative procedure. Each model is defined by a set of distinct parameter values to be matched. For the accurately known $M_{\rm J}, R_{eq}, \omega, J_2$, these values are the observed ones within an error of one standard deviation (1σ); for the less accurately known $\bar{Y}$ and J_4, the values are chosen in the 1σ range with a computational error of less than 10% of their 1σ error. The interior models are not optimized to meet J_6. Resulting values of J_6 lie always in the 1σ range, if J_2 and J_4 do. For a H-EOS with PPT, the transition pressure $P_{\rm m}$ from the molecular to the metallic layer is chosen to coincide with the entry of the outer isentrope into the instability region. For a H-EOS without PPT, the pressure is varied between 1.4 and 5 Mbar. For a distinct choice of mass fractions X of hydrogen, Y of helium, Z of metals, the EOS of the mixture is calculated, see §3.6. From these tabulated thermal and caloric EOS of the mixture, the entropy can be calculated via thermodynamic relations. The isentropes of the outer and of the inner envelope and the isotherm of the core are defined by the boundary conditions

(T_1, P_1), $(T_\mathrm{m}, P_\mathrm{m})$, and $(T_\mathrm{c}, P_\mathrm{c})$, where the transition temperature T_m results from the outer isentrope at $P = P_\mathrm{m}$, and the core temperature T_c from the inner isentrope at $P = P_\mathrm{c}$. Since the size of the core is not known in advance, P_c is varied within the iteration scheme described below until the total mass condition holds. Along this curve of piecewise constant entropy or temperature the equation of motion describing hydrostatic equilibrium,

$$\rho^{-1}\nabla P = \nabla(V + Q)\,, \tag{1}$$

is integrated inwards, where ρ is the mass density and $U = V + Q$ the total potential composed of the gravitational potential

$$V(\vec{r}) = G\int d^3r'\,\frac{\rho(\vec{r}\,')}{|\vec{r}\,' - \vec{r}|} \tag{2}$$

and the centrifugal potential Q defined by

$$-\nabla Q(\vec{r}) = \vec{\omega}\times(\vec{\omega}\times\vec{r})\,. \tag{3}$$

A proper description for the potential of axisymmetric but, due to rotation, oblate planets is a multipole expansion, which transforms the general expressions (2) and (3) into the following forms with spherical coordinates r, θ, and Legendre polynomials $P_{2n}(t = \cos\theta)$

$$V(r,\theta) = \frac{G}{r}\sum_{n=0}^{\infty} P_{2n}(t)\int d^3r'\,\rho(r',\theta')\left(\frac{r'}{r}\right)^{2k} P_{2n}(t')\,, \tag{4}$$

$$Q(r,\theta) = \frac{1}{3}\omega^2 r^2\left(1 - P_2(t)\right)\,. \tag{5}$$

The index $k = n$ describes the external gravitational potential for $r > r'$ and $k = -(n+1)$ the internal gravitational potential for $r < r'$. At the surface, the internal gravitational potential vanishes and V reduces to

$$V(r,\theta) = \frac{GM}{r}\left(1 - \sum_{n=0}^{\infty}\left(\frac{R_{eq}}{r}\right)^{2n} J_{2n}P_{2n}(t)\right)\,, \tag{6}$$

with the gravitational moments

$$J_{2n} = \frac{1}{MR_{eq}^{2n}}\int d^3r'\,\rho(r',\theta')r'^{2n}P_{2n}(t')\,. \tag{7}$$

Calculating the integrals in equations (4) and (7) requires knowledge of the planetary shape and the density distribution. We apply the *Theory of Figures* (Zharkov & Trubitsyn 1978) and the method described therein and in (Nettelmann et al. 2007) for solving the system of

integral equations on computers to iteratively calculate the planetary shape, the potential, and the density distribution. The key point of this theory is to reduce the dimension of the problem by replacing the former radial coordinate r by its representation

$$r(\theta) = l\left(1 + \sum_{i=0}^{\infty} s_{2i}(l) P_{2i}(t)\right) \tag{8}$$

on equipotential surfaces (l =const) with expansion coefficients $s_{2i}(l)$. Reasonable and practical cutoff indices for the sum in equation (8) are 3, 4 or 5. In accordance with the treatment of Guillot (1999a), we consider only coefficients up to third order, i.e. $i = 3$, which introduces an error into the calculation of the gravitational moments of the order of magnitude of J_6 or about five times the observational error of J_2. In terms of the level coordinate $l = 0 \ldots \bar{R}$, the equations to be integrated along the piecewise isentrope take the simple form

$$\frac{1}{\rho(l)} \frac{dP(l)}{dl} = \frac{dU(l)}{dl} \tag{9}$$

for the equation of motion and

$$\frac{dm}{dl} = 4\pi l^2 \rho(l) \tag{10}$$

for the equation of mass conservation. The mean radius $\bar{R}$ of the surface (at the 1-bar level) is not known in advance and has to be adjusted in order to satisfy $r(\theta = \pi/2) = R_{eq}$. The coefficients s_{2i} in equation (8), the *figure functions*, determine the shape of the rotating planet. As suggested by Zharkov & Trubitsyn (1978) they are calculated for a fixed density distribution $\rho(l)$ in an iterative procedure until convergence of at least 0.01% for s_2 is reached, which turns out to be accompanied by an error of 0.05% for s_4 and 0.1% for s_6. The converged figure functions enter into equations (9), (10), and (7) and a revised density distribution is calculated resulting in a different core mass and, thus, a different central pressure P_c. After about six iterations of calculating converged figure functions and corresponding density distributions, J_2 and J_4 are converged within their observational error bars, but not necessarily to the observed values $J_2^{\rm obs}$, $J_4^{\rm obs}$. To achieve agreement also with $\bar{Y}$, the guess of $Z_{\rm mol}$, $Z_{\rm met}$ and $Y_{\rm met}$ is improved slightly and the procedure decribed above is repeated, starting with the present density distribution, until the desired values of J_2, J_4 and $\bar{Y}$ have been approached. This procedure can, in principle, be applied to all giant planets in the Solar system.

2.3. Accuracy

In order to give reliable results for the interior structure model and to study the influence of different EOS data sets, the numerical treatment has to ensure a definite precision. The

accuracy of acceptable interior models should be in the order of or smaller than the relative error of the most accurate observed quantity to be adjusted during the procedure. For M_J, R_{eq} and J_2 the observational error is below 0.01% and for $\bar{Y}$, $Y_{\rm mol}$, T_1, and J_4 larger than 1%. The uncertainty associated with the QMD data themselves induces an error of the order of 1% to the isentropes. Hence we consider a numerical accuracy of 0.1% as sufficient to study the effect of the uncertainty of the less accurately known observables and for conclusive interior models regarding the EOS applied.

Numerical errors occur due to the integration of equations (9) and (10), the differentiation of the gravitational potential, and the integrals in equation (4), transformed to the level coordinate l. We have tested the accuracy of integrating the differential equations (9) and (10) for a non-rotating polytrope of index 1. Our numerical results for the profiles $m(r)$ and $P(r)$ obtained via a fourth-order Runge-Kutta method with adaptive stepsize control in regions with steep gradients differ by less than 0.001% from the analytical solution in the outer 80% of the planet. In the inner 20% of the planet including the core region, a shooting splitting method is applied to localize the outer boundary of the core. We then search for a solution starting from the center to meet the envelope solution there with a deviation of less than 0.1%. Since a polytropic model does not have a core, this method cannot be applied there and the difference rises to 50% for the mass and 0.1% for the pressure near the center.

To estimate the error resulting from the calculation of the integrals and its enhancement during the iteration procedure, we have compared fully converged planetary models. The resulting mass fractions $Z_{\rm mol}$ and $Z_{\rm met}$ and the size of the core differ by less than 2% if the number of intervals dl' in the integrations is doubled. Since density discontinuities at layer boundaries are extended over a small but finite intervall, they do not cause numerical difficulties. Extending this intervall from 0.001 R_J to 0.01 R_J effects the resulting core mass by about 0.1 $M_\oplus$ and the heavy element abundance by about 2%.

We conclude that a convergence of our numerical procedure within 0.1% can be ensured, but the resulting values for the model parameters are uncertain within ± 0.1 $M_\oplus$ or 2%.

3. EOS data

Interior models of Jupiter's present state require EOS data for H, He, and metals from about 160 K at 1 bar up to 25000 K at about 45 Mbar, and for core materials (rocks, ices) of 35-80 Mbar around 20000 K. No state-of-the-art thermodynamic model is capable of calculating accurate EOS data for all planetary materials in this wide pressure-temperature range. However, various EOS data sets have been constructed for this purpose by adopting

known limiting cases and interpolating in between or extending them till phase boundaries. Examples are the Sesame EOS data tables 5251, 5761 and 7150 for H, He and H_2O (SESAME library 1992) and chemical models such as the SCvH EOS (Saumon et al. 1995) and FVT^+ (Holst et al. 2007). These data sets have the largest uncertainties in the WDM regime. We have, therefore, performed extensive QMD simulations to generate accurate EOS data for warm dense H, He and H_2O, i.e. for moderate temperatures and densities higher than 0.2 (H, He) or 1 g cm^{-3} (H_2O). The new ab initio data cover at least 97% of the planetary material inside Jupiter. For lower densities, the simulation times increases dramatically so that other methods have to be applied.

We outline the method of QMD simulations below and describe the construction of improved EOS tables for H, He, and H_2O by combining QMD results for WDM with chemical models in complementary regions of the phase diagram. Predictions of these new EOS tables are compared with SCvH EOS with respect to the Jupiter adiabat and plasma parameters.

3.1. QMD simulations

For the QMD simulations we have used the code VASP (Vienna Ab Initio Simulation Package) developed by Kresse & Hafner (1993a,b) and Kresse & Furthmüller (1996). Within this method, the ions are treated by classical molecular dynamics simulations. For a given ion distribution, the density distribution of the electrons is determined using finite temperature density functional theory (FT-DFT). The electronic wave functions are represented by plane waves and calculated using projector augmented wave (PAW) pseudopotentials (Blöchl 1994; Kresse & Joubert 1999; Desjarlais et al. 2002). The central input into DFT is the exchange-correlation functional accounting for interactions between electrons and ions and the electrons themselves. It is calculated within generalized gradient approximation (GGA) using the parametrization of Perdew et al. (1999).

The convergence of the thermodynamic quantities in QMD simulations is an important issue. We found that a plane wave cutoff energy of 700 (He), 900 (H_2O, see Mattsson & Desjarlais (2006)), and up to 1200 eV (H, see Desjarlais (2003)) is necessary to converge the pressure within 3% accuracy. Furthermore, we have checked the convergence with respect to a systematic enlargement of the **k**-point set in the representation of the Brillouin zone. Higher-order **k** points modify the EOS data only within 1% relative to a one-point result. Therefore, we have restricted our calculations to the Γ point for water or the mean value point $(1/4, 1/4, 1/4)$ (Baldereschi 1973) for H and He. The overall uncertainty of the QMD data due to statistical and systematic errors is below 5%. The simulations were performed for a canonical ensemble where the temperature, the volume of the simulation box, and the

particle number in the box are conserved quantities. We consider 32 to 162 atoms in the simulation box and periodic boundary conditions. The ion temperature T_i is regulated by a Nosé-Hoover thermostat (Nosé 1984) and the electron temperature (with $T_e = T_i$) is fixed by Fermi weighting the occupation of bands using Mermins approach (Mermin 1965). At high temperatures, the number of bands to be considered increases exponentially with the electron temperature so that a treatment of high-temperature plasmas is rather challenging. However, simulations of WDM states at several 1000 K as typical for planetary interiors are performed without any serious difficulties. When the simulation has reached thermodynamic equilibrium, the subsequent 500 to 2000 time steps are taken to calculate the EOS data as running averages.

3.2. Construction of the hydrogen EOS

For densities below 0.1 g cm^{-3} we have used FVT$^+$ which treats the dissociation of molecules self-consistently and takes into account the ionization of the hydrogen atoms via a respective mass action law (Holst et al. 2007). FVT$^+$ makes use of Padé formulas (Chabrier & Potekhin 1998) for the plasma properties. Below 3000 K ionization does not play a role at planetary pressures and is thus neglected. FVT$^+$ data on the one hand and QMD data on the other hand are then combined within a spline interpolation.

Both methods yield different reference values U_0 for the internal energy, which have been fixed by the Hugoniot starting point of fluid, molecular hydrogen at 19.6 K and 0.0855 g cm^{-3}. The energy difference is added to the QMD data in order to get a smooth transition between the data sets. The final hydrogen EOS is referred to as *H-REOS*. Examples of isotherms are shown in Fig. 1.

3.3. Construction of the helium EOS

The He-EOS named *He-REOS* is a combination of QMD data for densities between 0.16 and 10 g cm^{-3} and temperatures between 4000 and 31600 K, and Sesame 5761 data (SESAME library 1992) for densities below 0.01 and above 16 g cm^{-3} and for lower and higher temperatures. For intermediate densities, the isotherms of both data sets were interpolated. In Fig. 2 we compare isotherms of He-REOS with Sesame 5761. QMD data for helium indicate a slightly lower compressibility around 1 Mbar. Optical properties, especially the metallization of fluid helium, as relevant for giant planets and white dwarf atmospheres have been investigated recently (Kietzmann et al. 2007; Kowalski et al. 2007) by means of QMD simulations.

3.4. Construction of the water EOS

The EOS of water named *H_2O-REOS* is a combination of four EOS data sets. QMD data are considered for $1000 \leq T \leq 10000$ K and between 2 and 7 g cm^{-3}, as well as for $10000 \leq T \leq 24000$ K and between 5 and 15 g cm^{-3}. Details of the QMD simulations for H_2O and the respective EOS data will be published elsewhere (French et al. 2008). For the phases ice I and liquid water we apply accurate data tables named *FW* (Feistel & Wagner 2006) and *WP* (Wagner & Prusz 2002), respectively. All other regions are filled up with Sesame 7150 data (SESAME library 1992). Intermediate EOS data are gained via interpolation.

Fig. 3 shows six pressure isotherms for H_2O-REOS representing different phases of H_2O and the pressure-density relation of the water fraction representing heavy elements along a typical Jupiter isentrope. Due to the phase diagram of pure H_2O, in the outermost region of Jupiter the H_2O-component transits from ice I to liquid water below 300 K and further to the vapor phase around 550 K. At about 4000 K, H_2O again reaches densities of 1 g cm^{-3} along the Jupiter isentrope. Above this point, water shows strong molecular dissociation and becomes also electronically conductive (Mattsson & Desjarlais 2006). From here on, the EOS of the water component in Jupiter is described by our QMD data. Following the isentrope further into the deep interior, water remains in the fluid, plasma-like phase.

Our H_2O phase diagram smoothly adds to recent QMD simulations by Mattsson & Desjarlais (2006). The EOS data differ at densities between 3-10 g cm^{-3} from the pure Sesame EOS.

3.5. EOS of metals and core material

We make use of the EOS table for water to represent metals in the envelopes. Alternatively, the EOS table of helium scaled in density by a factor of 4 (He4) is used to represent the atomic weight of oxygen. Oxygen is the third abundant element in the sun and probably also in Jupiter, see Kerley (2004a) for a discussion. We compare the respective isotherms of the EOS for metals in Fig. 4 in that density and temperature region where QMD data of H_2O are applied. The H_2O pressures are up to 10 times higher than the He4 data, probably resulting from enhanced ideal and pronounced Coulomb contributions in water plasma.

Previous models of Jupiter assumed that the core consists of rocks surrounded by ices (Chabrier et al. 1992; Gudkova & Zharkov 1999; Stevenson 1982). Traditionally, rock material is a mixture of S, Si, Mg, and Fe while ice refers to a mixture of C, N, O, and H. Due to the core accretion scenario for the formation process of giant planets (Alibert et al. 2004; Pollack et al. 1996), these elements have mainly entered the planetary interior in form of icy compounds of CH_4, NH_3, H_2O, and of porous material composed of SiO_2, MgO, FeS,

and FeO. Their present state in the deep interior of the planet cannot be inferred from observations or interior model calculations. Our QMD simulations show clearly that H_2O is in a plasma and not in a solid phase at conditions typical for the core of Jupiter (French et al. 2008). Since CH_4 and NH_3 are more volatile than H_2O, they are expected to prefer the plasma phase too in the core region of Jupiter. Because a smaller-sized core results from interior models rather than from formation models of Jupiter, the core has been argued to erode with time (Alibert et al. 2004; Guillot et al. 2003). Motivated by the possibility of core erosion and by the miscibility of the icy component within the metallic envelope we assume that the core consists purely of rocks in all our calculations for Jupiter. The EOS of rocks is adapted from Hubbard & Marley (1989).

3.6. Mixtures

The EOS of a mixture with mass fractions X of hydrogen, Y of helium, and Z of metals is calculated by means of the EOS for the pure components using the additive volume rule (Chabrier et al. 1992; Peebles 1964) for the internal energy,

$$u(P,T) = Xu_X(P,T) + Yu_Y(P,T) + Zu_Z(P,T)\,, \tag{11}$$

and the mass density,

$$\frac{1}{\rho(P,T)} = \frac{X}{\rho_X(P,T)} + \frac{Y}{\rho_Y(P,T)} + \frac{Z}{\rho_Z(P,T)}\,, \tag{12}$$

on a grid of pressures P and temperatures T. Non-ideality effects of mixing are thus not taken into account.

In this paper we refer to three different linear mixtures of EOS data abbreviated by *LM-REOS*, *SCvH-ppt* and *SCvH-i*. The new data set *LM-REOS* consists of a linear mixture as described above of H-REOS, He-REOS, and of H_2O-REOS or He4-REOS for metals. *SCvH-ppt* as used in this work consists of H-SCvH-ppt for hydrogen and He-SCvH for helium (Saumon et al. 1995), and of He-SCvH scaled in density by a factor four as representative for metals. *SCvH-i* as used in this work consists of the interpolated version (Saumon et al. 1995) of H-SCvH-ppt together with the same EOS for He and metals as for SCvH-ppt. Apart from SCvH-ppt, none of the hydrogen or helium EOS used here shows a first-order phase transition.

For given mixtures, the piecewise isentrope defined by the boundary condition is calculated as described in §2.2. When using H_2O for metals we make the following exception for temperatures below 1000 K. At these small temperatures where H_2O passes the phases

ice I, liquid water, and vapor, we first calculate the isentrope of the H/He mixture and then add the desired mass fraction of H_2O to the $P-\rho$ relation of that isentrope according to its $P-T$ relation. At 1000 K, the pieces of isentropes for smaller and higher temperatures add very smoothly, as can be seen from Fig. 3.

3.7. Comparison with chemical models

Results of our LM-REOS for the coupling parameter Γ, the degeneracy parameter Θ, and the pressure-density relation along the hydrogen adiabat are compared with the chemical models SCvH-ppt and SCvH-i.

We have applied the definition of Γ and Θ given by Chabrier & Potekhin (1998) for multi-component plasmas with mean ion charge $\langle Z \rangle$ and electron density n_e

$$\Gamma = \frac{e_0^2}{4\pi\epsilon_0 k_B} \left(\frac{4\pi}{3}\right)^{1/3} \times \frac{\langle Z \rangle^{5/3} n_e^{1/3}}{T} \tag{13}$$

$$\Theta = \frac{k_B}{\hbar^2} 2m_e (3\pi)^{2/3} \times \frac{T}{n_e^{2/3}} \,. \tag{14}$$

These plasma parameters are calculated along typical Jupiter adiabats by taking into account the ionization degree of hydrogen and helium. For models with the SCvH-ppt and SCvH-i EOS, the fraction of H^+, He^+, and He^{2+} was taken simply from their tables. This is not directly possible for models using the QMD data sets because the underlying strict physical picture does not discriminate between bound and free states. However, we have estimated the ionization degree of the He component by using the COMPTRA04 program package (Kuhlbrodt et al. 2005). In the underlying chemical model of COMPTRA04, the composition of a partially ionized plasma at a given temperature and mass density is determined by the solution of coupled mass action laws including non-ideal contributions to the chemical potential via Padé-formulas and a polarization potential accounting for the interaction between electrons and neutral atoms. For the hydrogen subsystem, the degree of dissociation is evaluated via the proton-proton distribution function and the coordination number derived from the QMD runs; this method is described in more detail by Holst et al. (2008). According to state-of-the-art chemical models for hydrogen such as SCvH or FVT^+, the fraction of atoms is always small so that we can estimate the ionization degree in the hydrogen component by taking the dissociation degree as an upper limit. Results for Γ and Θ are shown in Fig. 5 as function of the mass coordinate in Jupiter.

At least 80% of Jupiter's mass is in a state with strong coupling and degeneracy effects, defined by $\Gamma > 1$ and $\Theta < 1$. With SCvH-ppt, the step-like increase of Γ coincides with the

density discontinuity at the layer boundary. LM-REOS has a much earlier onset of ionization in the hydrogen component than both SCvH-ppt and SCvH-i. In the very deep interior, only about 5% of the He atoms are singly ionized and less than 1% doubly ionized as inferred from the chemical model COMPTRA04 applied to our LM-REOS data, while complete ionization is predicted by the SCvH-He EOS so that Γ becomes slightly larger in that models. This large discrepancy between chemical models in the region of pressure ionization is due to a different treatment of correlation effects occuring in the exponents of the mass-action laws for ionization, from which the composition is derived. Higher temperatures as with the SCvH-ppt EOS diminish the degeneracy and in spite of fully ionized helium the same values are found as with LM-REOS.

More than 50% of Jupiter's mass is in a high-pressure state between 0.1 and 10 Mbar where the differences in the hydrogen isentropes are most pronounced and manifest themselves in the structure models, see §4.2. With the transition from FVT^+ data to QMD data around 0.05 Mbar, the Jupiter isentrope of pure hydrogen becomes much softer than H-SCvH-i, with a maximum difference of 30% at 1 Mbar, as shown in Fig. 6. In the innermost 20% of Jupiter's mass, i.e. above 20 Mbar, the H-REOS isentrope follows the H-SCvH-ppt one with 5% higher pressures than SCvH-i. Differences below 0.1 Mbar do not significantly contribute to the structure models since this region occupies less than 2% of Jupiter's total mass.

4. Results for Jupiter

In this section we present results for Jupiter's core mass, for the abundances of metals in the envelopes, and for the profiles of the main components along the radius. The size of the core M_c determined by the condition of total mass conservation, and the abundances of metals Z_{mol}, Z_{met} which are needed to reproduce J_2 and J_4 are very sensitive with respect to the choice of the EOS and the precise values of the observational parameters to be reproduced. First, we compare our results with those of Guillot et al. (2003) by using the same EOS data sets (SCvH-ppt and SCvH-i) in order to demonstrate that our procedure is sound. In §4.2 we then present the range of acceptable Jupiter models using our new LM-REOS in comparison with SCvH-based models, explore in §4.3 the behavior of LM-REOS based models by varying T_1, J_4, and P_{m}, and discuss in §4.4 the fractions of chemical species calculated with LM-REOS and SCvH-ppt for Jupiter models which satisfy the same observational constraints given in Tab. 1.

4.1. Consistency with former results

We follow the notation of Guillot et al. (2003) who has performed extensive calculations for planetary interiors and study four of the models he has introduced explicitly. These reference models (A, B, D, E)-TG are based on a three-layer structure as also adapted here. Tab. 2 contains their first independent confirmation. In our recalculated models labeled (A,..., E)-this, we do not allow for a deviation of $\bar{Y}$ and J_4 of more than $1/10\sigma$; but in our models labeled (A',..., E')-this, $\bar{Y}$ and J_4 are varied within 1σ in order to achieve the best agreement as possible. Corresponding numbers are listed in Tab. 3.

Table 2. Comparison of present (this) and former (TG) results.

Model	H-EOS SCvH-	T_1 [K]	M_c $[M_\oplus]$	M_Z $[M_\oplus]$	$Z_{\rm met}$ $[Z_\odot]$	$Z_{\rm mol}$ $[Z_\odot]$
A-TG	i	165	4.2	33.1	4.7	5.3
A-this	i	165	0.7	35.6	6.0	4.5
A'-this	i	165	2.8	34.2	5.2	5.0
B-TG	i	170	0	35.3	6.1	4.1
B-this	i	170	0.8	36.4	6.0	4.9
B'-this	i	170	0	35.5	6.0	4.8
E-TG	ppt	165	4.3	19.4	2.5	2.3
E-this	ppt	165	6.7	24.8	2.9	3.9
E'-this	ppt	165	4.6	22.7	2.9	3.3
D-TG	ppt	170	10.0	17.5	0.7	4.5
D-this	ppt	170	7.0	25.7	2.9	4.2
D'-this	ppt	170	8.6	22.6	1.9	4.9

Note. — The mass fraction of heavy elements is given in solar units $Z_\odot = 1.92\%$. Models (A–E)-TG are taken from Guillot et al. (2003). Present models with prime are designed to give the best agreement, see Table 3 for the choice of parameters.

Models (A–E)-TG indicate that T_1 affects M_c by several $M_\oplus$, but apparently not systematically. Keeping other constraints constant, we always find a slightly higher core mass for a larger 1-bar temperature. On the other hand, shifting the layer boundary between the envelopes outwards, e.g. from 2.0 to 1.4 Mbar in model A'-this, always magnifies the core mass such that the result $M_c(A) > M_c(B)$ of Guillot et al. (2003) can be reproduced. Our value of $M_c = 2.8\ M_\oplus$ in model A'-this can be further increased by $0.6\ M_\oplus$ if we use ices as core material instead of rocks.

Table 3. Parameters of present Jupiter models using SCvH EOS

Model	$P_{\rm m}$ [Mbar]	$\bar{Y}$ [%]	$J_4/10^{-4}$
A&B-this	2.00	27.5	-5.84
E-this	1.73	27.5	-5.84
D-this	1.76	27.5	-5.84
A'-this	1.40	28.0	-5.89
B'-this	2.00	27.8	-5.82
E'-this	1.77	28.5	-5.79
D'-this	1.74	28.5	-5.89

Note. — In models using SCvH-ppt EOS, $P_{\rm m}$ coincides with the PPT. These models have been calculated in order to check the consistency with former results, see Table 2.

In agreement with Guillot et al. (2003) the total abundance of metals $M_Z = M_{Z_{\rm mol}} + M_{Z_{\rm met}} + M_c$ increases by 10-15 $M_\oplus$ when using SCvH-i instead of SCvH-ppt. Since all our solutions yield $Z_{\rm mol} < Z_{\rm met}$ with SCvH-i and $Z_{\rm mol} > Z_{\rm met}$ with SCvH-ppt in agreement with the bulk of solutions in Guillot et al. (2003), the inverse ratio of models A-TG and E-TG cannot be reproduced. Apart from the deviations of 43% for $Z_{\rm mol}$(E') and 170% for $Z_{\rm met}$(D'), the deviations of all other solutions are below 30% so that they lie within the range of solutions found in Guillot et al. (2003). With $0 < M_c < 10$, $17.5 < M_Z < 35.3$, $2.3 < Z_{\rm mol} < 5.3$, and $0.7 < Z_{\rm met} < 6.1$ the solutions (A–E)-TG span large ranges in units of Earth masses and solar abundances $Z_\odot = 1.92\%$, respectively. Our nearest results differ by up to 1.4 $M_\oplus$ for M_c, 5.1 $M_\oplus$ for M_Z, 1.0 $Z_\odot$ for $Z_{\rm mol}$, and 1.2 $Z_\odot$ for $Z_{\rm met}$ from these results. To reduce the disagreement in model D with respect to $Z_{\rm met}$ and M_Z, which are nearer to model E-TG than to D-TG, the mean helium content should be higher or the EOS of metals be more compressible.

We conclude that our method is able to reproduce former results well enough to smoothly continue and complement investigations of the interplay between the internal structure of giant planets and the EOS applied.

4.2. New results with LM-REOS

Figures 7 and 8 show the full range of solutions using QMD data in comparison with models based on SCvH-ppt and SCvH-i adapted from Guillot et al. (2003) with respect to M_c, M_Z, $Z_{\rm mol}$, and $Z_{\rm met}$. Figures 9 and 10 illustrate the effect of a varying $P_{\rm m}$, T_1, and J_4 on the position of the QMD data based solutions. For all our solutions, $Y_{\rm mol} = 0.238$, $\bar{Y} = 0.275$, $P_{\rm m}$ is varied from 3 to 5 Mbar, T_1 from 165 to 170 K and J_4 from -5.84 to -5.89$\times 10^{-4}$. Metals are represented either by He4 or by H_2O, see §3.5.

The behavior of the isentropes already indicates (see Fig. 6) that the solutions based on LM-REOS are nearer to the SCvH-i than to the SCvH-ppt results. This is a clear consequence of the missing PPT in the H-REOS data. The PPT makes the H-EOS less compressible in the molecular regime and more compressible in the metallic regime before it is dominated by electronic degeneracy.

The core mass of QMD-based models does not vanish for transition pressures up to 5 Mbar and $J_4 \leq J_4^{\rm obs}$. On the other hand, the core mass of our SCvH-i models does not exceed 4 $M_\oplus$ at transition pressures as low as 1 Mbar. Higher core masses could be achieved with SCvH-i for $P_{\rm m} < 1$ Mbar, but are not reasonable since the layer boundary is to represent the PPT which occurs above 1 Mbar for SCvH-ppt. Higher core masses of

QMD-based models can be explained by a smaller compressibility at pressures above 10 Mbar as seen from the isentropes. For a given abundance of metals, a smaller compressibility of hydrogen adds less mass to the isentrope and leaves more mass for the core. Similary, the smaller the compressibility of the EOS of metals (Fig. 4), the higher their abundance needed to contribute mass to the isentrope in order to match J_2 and J_4.

A pronounced difference between the isentropes calculated with the LM-REOS and SCvH-i occurs around 1 Mbar, where the QMD pressure is up to 30% smaller. This feature leads to smaller $Z_{\rm mol}$ and higher transition pressures, see Fig. 8, which can be explained as follows. For a given pressure-density relation along the isentrope as required by equations (9) and (7), a higher compressibility of the hydrogen component has to be compensated by a smaller metal abundance in order to keep J_2 and J_4 at the observed values. Guillot (2005) has also shown that the mean radius of the contribution of level radii to the gravitational moments J_{2n} increases with increasing index n and is placed around the layer boundary in case of J_2 and J_4, whereas the contribution to higher moments than J_2 from the deep interior is negligible. The molecular region contributes slightly more to J_4 than to J_2, and the metallic layer contributes slightly more to J_2 than to J_4. If the compressibility of hydrogen becomes large near the molecular-metallic layer boundary, $Z_{\rm mol}$ has to be chosen small in order to not exceed $|J_4|$; but simultaneously J_2 will become too low and thus $Z_{\rm met}$ has to be enhanced strongly, again enlarging simultaneously $|J_4|$ beyond the desired value. Therefore, in order to adjust both gravitational moments with a $Z_{\rm mol}$ not too small, the influence of $Z_{\rm met}$ on J_4 has to be reduced by shifting the layer boundary inwards. LM-REOS based models of Jupiter have $Z_{\rm mol} = 0.2 - 1.8\,Z_\odot$, $Z_{\rm met} = 4.8 - 9.6\,Z_\odot$ for $P_{\rm m} = 3$ to 5 Mbar.

4.3. Systematic behavior of LM-REOS solutions

In this paragraph we illustrate the influence of the uncertainties in observational and free parameters on the position of the solution of LM-REOS based models in the usual M_c vs. M_Z and $Z_{\rm mol}$ vs. $Z_{\rm met}$ diagrams. For our point of reference, displayed as filled circle in Figs. 9 and 10, we have chosen the values $J_4/10^{-4} = -5.84$, $T_1 = 170$ K, and $P_{\rm m} = 4$ Mbar. As explained above, $Z_{\rm mol}$ increases with $|J_4|$. We do not consider solutions for $|J_4|/10^4 < 5.84$ since they result in $Z_{\rm mol} < Z_\odot$ or $M_c = 0$. In the molecular envelope where the isentrope is more sensitive with respect to temperature than in the degenerate metallic region, a cooler interior initiated by a smaller T_1 enhances the partial density of the He-H mixture and reduces the fraction of metals by 1 $M_\oplus$. Most important, the solutions are affected by the choice of the transition pressure. For $P_{\rm m} < 3$ Mbar, no solution exists with $Z_{\rm mol} > Z_\odot$. Solutions with $1 < Z_{\rm mol} < 1.8 \times Z_\odot$ are found for $3 < P_{\rm m} < 5$ Mbar in combination with

$T_1 = 170$ K and $J_4 \leq -5.84 \times 10^{-4}$. A slightly higher enrichment factor of 2.0 is possible for $P_\mathrm{m} = 7$ Mbar, before the core mass shrinks to zero. In contrast to the large influence of P_m on Z_mol and Z_met, M_Z just varies within one $M_\oplus$. Finally, representing metals by H_2O instead of He4 enhances Z_met by 50% and shifts M_Z from about 30 to about 40 $M_\oplus$.

4.4. Profiles of chemical components

We compare the abundances of single chemical species, see §3.7, along the radius inside Jupiter as calculated with LM-REOS (model J11a in Fig. 11, corresponding to the point of reference for H_2O in Fig. 9) and with SCvH-ppt (model J11b in Fig. 11). In these figures, a full arc segment corresponds to 100% in mass. The radius coordinate is not displayed here but scales linearly from the center to the pressure level of 1 bar. In both of the models the core consists of rocks, $J_4/10^{-4} = -5.84$, $\bar{Y} = 27.5\%$, and $T_1 = 170$ K. There is no degree of freedom in model J11b and the only degree of freedom in model J11a, P_m, is set to 4 Mbar in order to give $Z_\mathrm{mol} > 1$. The three most important differences are: (i) the steep onset of dissociation and ionization of H-atoms with the PPT in model J11b wheras LM-REOS yields a smooth increase of dissociation; (ii) a high transition pressure of 4 Mbar in model J11a, well beyond the location of the PPT in SCvH-ppt; (iii) a ratio of heavy elements Z_mol:Z_met of 4:3 in model J11b compared to 1:6 with LM-REOS. It is interesting to note that once neutral H and He^+ are formed in the SCvH-ppt model, they are almost immediately ionized further, whereas the fraction of ionized He of only 6% in the deep interior in model J11a is not resolved.

For model J11a, an ASCII data table containing the profiles of pressure, temperature, density, composition and the figure functions along the radius is availiable in the electronic edition of this Journal. A shortened version of this data table is shown in Tab. 4, where the five rows, from top to bottom, present the 1-bar-level surface, the transition from the outer to the inner envelope, and the layer transition from the inner envelope to the core.

Table 4. Jupiter model J11a

m [$M_\oplus$]	P [Mbar]	l [$\bar{R}_J$]	T [K]	ρ [g cm^{-3}]	Y [%]	Z [%]	X_{H_2}	X_{He}	X_{He+}	s_2	s_4	s_6
317.8336	1.0000E-06	1.00000	1.7000E+02	1.6653E-04	23.307	2.072	1.0000	1.0000	0.0000	-4.501E-02	1.984E-03	-2.470E-04
⋮	⋮	⋮	⋮	⋮	⋮	⋮	⋮	⋮	⋮	⋮	⋮	⋮
223.6070	3.9998E+00	0.72384	8.8682E+03	1.3239E+00	23.307	2.072	0.0095	1.0000	0.0000	-3.522E-02	1.062E-03	-1.742E-04
223.5810	4.0013E+00	0.72380	8.8694E+03	1.5253E+00	24.476	16.616	0.0095	1.0000	0.0000	-3.522E-02	1.062E-03	-1.744E-04
⋮	⋮	⋮	⋮	⋮	⋮	⋮	⋮	⋮	⋮	⋮	⋮	⋮
2.75441	3.8385E+01	0.08426	1.8571E+04	4.3293E+00	24.476	16.616	0.0000	0.9405	0.0574	-1.160E-02	1.063E-04	-7.278E-06
2.75308	3.8393E+01	0.08426	1.8572E+04	1.8037E+01	0.000	0.000	0.0000	0.0000	0.0000	-1.160E-02	1.063E-04	-7.278E-06

Note. — This table is a truncated version of a machine-readable table that is published in its entirety in the electronic edition of the Astrophysical Journal. Column headings from left to right: mass coordinate, pressure, level coordinate (radius, see Eq. 8), temperature, mass density, mass fraction of helium, mass fraction of metals (H_2O), particle fraction of H_2 molecules with respect to the H subsystem, particle fraction of neutral He (column 9) and of singly ionized He (column 10) with respect to the He subsystem, and columns 11-13: the dimensionless figure functions s_2, s_4, s_6.

5. Evaluation of the new results

In this chapter we discuss to what extent the new results for M_c, $Z_{\rm met}$, $Z_{\rm mol}$, and $P_{\rm m}$ obtained by using LM-REOS are in agreement with experimental EOS data (e.g. principal Hugoniot curve), evolution theory, element abundances, and H/He phase separation.

5.1. Core mass M_c

Saumon & Guillot (2004) found that H-EOS with a small maximum compression ratio of only 4 along the Hugoniot curve can yield small core masses lower than 3 $M_\oplus$ and comment that the apparent relation between the stiffness along the principal Hugoniot and the core mass may be not unique. In the same sense, our H-REOS reproduces the maximum compression ratio of 4.25 as derived from shock-wave experiments, but the core masses range up to 7 $M_\oplus$.

To understand the indirect effect of the compressibility κ of hydrogen on the core mass, we study in particular its impact in the deep interior ($\kappa_{\rm met}$), around the layer boundary between the envelopes ($\kappa_{\rm m}$), and in the outer molecular region ($\kappa_{\rm mol}$). The core mass depends essentially and directly on the mass density $\rho_{\rm met}$ in the deep interior: The higher $\rho_{\rm met}$, the lower $M_{\rm c}$. Clearly, $\rho_{\rm met}$ can either be enhanced by $\kappa_{\rm met}$ or by $Z_{\rm met}$. For example, the case of a smaller $\kappa_{\rm met}$ leading to a smaller $\rho_{\rm met}$ occurs with LM-REOS. Furthermore, $Z_{\rm met}$ is diminished by both $\kappa_{\rm m}$, which reduces the need for metals in order to adjust J_2, and the $Z_{\rm mol}$ chosen to reproduce J_4. Finally, $Z_{\rm mol}$ decreases with $\kappa_{\rm mol}$, for instance in case of SCvH-ppt. Due to this propagation of effects, the behavior found in Saumon & Guillot (2004) may correspond to the coincidence of a small $\kappa_{\rm m}$ and a large $\kappa_{\rm met}$ between 5-15 Mbar, see Fig. 1 in Saumon & Guillot (2004). In agreement with Saumon & Guillot (2004) we conclude that the compressibility along the principal Hugoniot curve, which is restricted to densities below about 1 g cm^{-3}, does not determine the core mass alone. Experimental data for the hydrogen EOS off the principal Hugoniot curve, i.e. near the isentrope, are in this context urgently needed. For this, new experimental techniques such as reveberating shock waves or precompressed targets can be applied.

5.2. Abundance of metals $Z_{\rm met}$

In our new Jupiter models with LM-REOS, $Z_{\rm met}$ is enriched over solar abundance by a factor of 5 to 10 and exceeds $Z_{\rm mol}$ by a factor of 4 to 30. This feature is consistent with the standard giant planet formation scenario, the core accretion model (Alibert et al. 2005;

Pollack et al. 1996), where the planet grows first by accretion of planetesimals onto a solid core embryo. If the core has grown such that surrounding nebula gas is attracted, an envelope forms and the planet grows by accretion of both gas and planetesimals, either sinking towards the core (Pollack et al. 1996) or dissolving in the envelope. If the luminosity of the envelopes has reached a critical value, the energy loss due to radiation cannot be supplied anymore by infalling planetesimals, and the whole planet starts to contract with an even enhanced gas accretion rate (run-away growth). Depending on a variety of parameters described in detail in Alibert et al. (2005), at the end of the lifetime of a protoplanetary disk a Jupiter-mass giant planet may have formed with a core mass of several $M_\oplus$ and a total mass of heavy elements of 30-50 $M_\oplus$. Further evolution of the planet may include erosion of core material (Chabrier & Baraffe 2007; Guillot et al. 2003) and homogeneous redistribution of destroyed planetesimals due to convection (Kerley 2004a). Both of these processes depend on the ability of convection to overcome compositional gradients and their efficiency is not known in detail up to now (Chabrier & Baraffe 2007; Guillot et al. 2003). Thus, in the framework of the core accretion model, the distribution of heavy elements in our Jupiter models can qualitatively be explained as a consequence of planetesimal deliveries in the deep interior and their redistribution within the metallic layer by convection.

5.3. Abundance of metals $Z_{\rm mol}$

With the exception of oxygen, measurements of the abundance of the elements C, N, S, P and the noble gases beside He and Ne give two- to fourfold enrichment over solar abundance (see Guillot (2005) for an overview). On the other hand, the Galileo probe gave an O/H ratio of only $0.2 \times Z_\odot$. It has been argued that the probe fell into a non-representative dry region and the O abundance was still rising with depth when the probe stopped working (Kerley 2004a). Our result of $Z_{\rm mol} = 1 - 1.8 \times Z_\odot$ is too low by a factor of two. We note that LM-REOS based three-layer Jupiter models are difficult to reconcile with the observed atmospheric abundances of heavy elements.

5.4. Layer boundary $P_{\rm m}$

None of the mechanisms known to affect $Z_{\rm mol}$, e.g. H/He phase separation or the properties of the nebula in the neighbourhood of the forming planet, could explain a depletion of heavy elements from the gas phase below solar abundance. To let the Jupiter models have $Z_{\rm mol} > Z_\odot$ requires $P_{\rm m} > 3$ Mbar using LM-REOS. In the three-layer model the discontinuity of the fraction of metals is assumed to occur at the same pressure as the discontinuity of the

fraction of helium. For helium, the discontinuity has been argued to coincide with a PPT of hydrogen or with the onset of H/He phase separation (Stevenson & Salpeter 1977b). Our QMD simulations show no indications of a PPT so far.

H/He phase separation on the other hand is a consequence of non-linear mixing and characterized by a line $T(x, P)$ of demixing which denotes for a certain concentration x the maximal, pressure-dependent temperature for which the system shows phase separation. While neutral He atoms are expected to separate from metallic hydrogen, ionized helium becomes miscible again at high pressures. However, only few theoretical results for the demixing line exist up to now. Latest simulations (Pfaffenzeller et al. 1995) have a line of demixing at temperatures well below the adiabatic temperature profiles of Jupiter and even of Saturn. Some theoretical EOS of H/He mixtures predict that the Jupiter isentrope intersects the high pressure boundary of the demixing line between 1.5 (Fortney & Hubbard 2004) and 7 Mbar (Stevenson & Salpeter 1977a). At smaller and at higher pressures along the isentrope, the system would mix again. These results are not confident enough to support or exclude a layer boundary around 4 Mbar.

5.5. Possible improvements

Three-layer models of Jupiter based on QMD data are consistent with the core accretion model, but cannot reproduce observed heavy element enrichments by a factor of 2 to 4. Transition pressures below 3 Mbar are even accompanied by $Z_{\rm mol} < 1\,Z_{\odot}$. Considering the agreement of our ab initio QMD results with measured Hugoniot curves and reflectivities for hydrogen, the present results for Jupiter point to the importance of three topics to be addressed in the future: (i) inclusion of mixing effects in the EOS instead of applying linear mixing, (ii) recalculation of the H/He demixing line within an ab initio approach; and (iii) adjustment of the structure model in order to account for phase boundaries of H/He demixing and He enrichment at deeper levels while still keeping the model as simple as possible.

First results on the effect of nonlinear mixing to the pressure-density relation were obtained by Vorberger et al. (2006) within DFT-MD simulations. They find that the volume at constant pressure is enhanced up to 5% at temperatures typical for the deep molecular layer where our H-EOS exhibits the highest compressibility, i.e. the smallest volume relative to SCvH-i. Taking into account the small mass fraction of metals, a compensation of a 2% density reduction in average of the H/He component in the outer envelope would require the fraction of metals to be doubled to about 3 $Z_{\odot}$ which is just the average of observed particle species. This effect is, therefore, a serious candidate to remove the mismatch between calculated and observed $Z_{\rm mol}$, see discussion above.

Using LM-REOS, the NMT in Jupiter occurs at 0.5 Mbar and is clearly separated from the layer boundary around 4 Mbar with about 80 $M_\oplus$ in between. If the order of the latter one will be confirmed by future work on the H/He phase diagram, the possibility of an extended inhomogenous layer enhancing the compressibility should be taken into account in the structure model.

In order to complement these and former investigations (e.g. Hubbard 1969; Saumon & Guillot 2004) of the interplay between the internal structure of giant planets and the EOS applied, a calculation of the evolution history including H/He phase separation is also necessary.

5.6. Impact for other planets

Corresponding results can be obtained also for Saturn, Uranus, and Neptune but with higher uncertainty regarding M_c, $Z_{\rm mol}$ and $Z_{\rm met}$. For most of the extrasolar giant planets (EGP) detected so far the only structural parameter constrained at all is the minimum mass. Transit detections also allow to determine the mean radius with an error of about 10% (Sato et al. 2005) resulting mainly from the uncertainty in the stellar radius. Even the few transiting planets detected so far have revealed a huge variety of mass-radius relationships. To explain them and to derive implications for their formation and contraction history, well-grounded knowledge of the Solar system giant planets is crucial. For instance, characteristics as helium depletion and compositional gradients are expected to apply also to EGPs (Chabrier & Baraffe 2007; Fortney & Hubbard 2004; Sato et al. 2005).

6. Conclusions

We have computed three-layer structure models of Jupiter using new EOS data for H, He, and H_2O. They are composed of ab initio data in the warm dense matter region covering at least 97% of Jupiter's total mass and of chemical model EOS at low densities. With 0 to 7 $M_\oplus$, the core mass compares with previous results satisfying the same observational constraints. Most of the other properties of QMD-based models such as (i) up to tenfold enrichment with heavy elements in the metallic layer, (ii) small heavy element abundance in the outer envelope, and (iii) a transition pressure of at least 3 Mbar, are a consequence of the high compressibility of the hydrogen EOS between 0.1 and 10 Mbar along the isentrope, but not along the Hugoniot. Transition pressures of 3 to 5 Mbar agree with estimates of the onset of remixing of hydrogen and helium that are demixing at smaller pressures.

These results clearly underline the importance of calculating the H/He phase diagram

with respect to the EOS and the region of helium immiscibility in order to improve our understanding of the internal structure of hydrogen-rich giant planets. These issues will be addressed in future work.

We thank J. Köhn, W. Lorenzen, T.R. Mattsson, I. Iosilevskiy, and T. Guillot for stimulating discussions and D. Saumon, G. Chabrier, and G. Kerley for providing us with their EOS data. The suggested corrections by the anonymous referee helped to improve the paper. This work was supported by the Deutsche Forschungsgemeinschaft within the Graduiertenkolleg GRK 567, the Sonderforschungsbereich SFB 652, and by the High Performance Computing Center North (HLRN) under contract mvp00006. We thank the Computing Center of the University of Rostock for assistance.

REFERENCES

Alibert, Y., Mordasini, C., & Benz, W. 2004, A&A, 417, L25

Alibert, Y., Mordasini, C., Benz, W., & Winisdoerffer, C. 2005, A&A, 434, 343

Atreya, S.K., Mahaffy, P.R., Niemann, H.B., Wong, M.H, Owen, T.C. 2003, Planet. Space Sci., 51, 105

Bahcall, J.N. 1995, Rev. Mod. Phys., 67, 781

Baldereschi, A. 1973, Phys. Rev. B, 13, 5188

Beule, D., Ebeling, W., Förster, A., Juranek, H., Redmer, R., & Röpke, G. 2001, Phys. Rev. E63, 060202

Bonev, S.A., Militzer, B., & Galli, G. 2004, Phys. Rev. B69, 014101

Boriskov, G.V., Bykov, A.I., Il'kaev, R.I., Selemir, V.D., Simakov, G.V., Trunin, R.F., Urlin, V.D., Shuikin, A.N., and Nellis, W.J. 2005, Phys. Rev. B, 71, 092104

Celliers, P.M., Collins, G.W., DaSilva, L.B., Gold, D.M., Cauble, R., Wallace, R.J., Foord, M.E., & Hammel, B.A. 2000, Phys. Rev. Lett., 84, 5584

Chabrier, G. & Baraffe, I. 2007, ApJ, 661, L81

Chabrier, G. & Potekhin, A.Y. 1998, Phys. Rev. E, 58, 4941

Chabrier, G., Saumon, D., Hubbard, W.B., & Lunine, J.I. 1992, ApJ, 391, 817

Collins, G.W. et al. 1998, Phys. Plasmas, 5, 1864

Collins, L.A., Bickham, S.R., Kress, J.D., Mazevet, S., Lenosky, T.J., Truiller, N.J., & Windl, W. 2001, Phys. Rev. B63, 184110

Desjarlais, M.P., Kress, J.D., & Collins, L.A. 2002, Phys. Rev. E, 66, 025401

Desjarlais, M.P. 2003, Phys. Rev. B68, 064204

Ebeling, W. & Norman, G. 2003, J. Stat. Phys., 110 861

Fortney, J.J. & Hubbard, W.B. 2004, ApJ, 608, 1039

Fortov, V.E., et al. 2007, Phys. Rev. Lett., 99, 185001

French, M., Redmer, R., & Mattsson, T.R. 2008, Phys. Rev. Lett., submitted

Gudkova, T.V. & Zharkov, V.N. 1999, Planet. Space Sci., 47, 1201

Guillot, T., Gautier, D., Chabrier, G., & Mosser B. 1994, Icarus, 112, 337

Guillot, T., Chabrier, G., Morel, P., Gautier, D. 1994, Icarus, 112, 354

Guillot, T. & Morel, P. 1995, A&AS, 109, 109

Guillot, T. 1999, Planet. Space Sci., 47, 1183

Guillot, T. 1999, Science 296, 72

Guillot, T., Stevenson, D.J., Hubbard, W.H., & Saumon, D. 2003, in Jupiter: The Planet, Satellites, and Magnetosphere, ed. F. Bagenal et al. (Cambridge, UK: Cambridge Univ. Press)

Guillot, T. 2005, Ann. Rev. Earth & Plan. Sci., 33, 493

Holmes, N.C., Ross, M., & Nellis W.J. 1995, Phys. Rev. B, 52, 15835

Holst, B., Nettelmann, N., & Redmer, R. 2007, Contrib. Plasma Phys., 47, 368

Holst, B., Redmer, R. & Desjarlais, M.P. 2008, Phys. Rev. B, accepted

Hubbard, W.B. 1968, ApJ, 152, 745

Hubbard, W.B. 1969, ApJ, 155, 333

Hubbard W.B. & Marley M.S. 1989, Icarus, 78, 102

Kerley, G.I. 2003, Sandia National Laboratories Report SAND2003-3613, Albuquerque/NM

Kerley, G.I., 2004, Kerley Technical Services Research Report KTS04-1, Appomattox/VA

Kerley, G.I., 2004, Kerley Technical Services Research Report KTS04-2, Appomattox/VA

Kietzmann, A., Holst, B., Redmer, R., Desjarlais, M.P., & Mattsson, T.R. 2007, Phys. Rev. Lett., 98, 190602

Klepeis, J.E., Schafer, K.J., Barbee, T.W., & Ross, M. 1991, Science, 254, 986

Kowalski, P.M., Mazavet, S., Saumon, D., & Challacombe, M. 2007, Phys. Rev. B, 76, 075112

Knudson, M.D., Hanson, D.L., Bailey, J.E., Hall, C.A., Asay, J.R., & Deeney, C. 2004, Phys. Rev. B, 69, 144209

Kresse, G. & Hafner, J. 1993, Phys. Rev. B, 47, 558;

Kresse, G. & Hafner, J. 1993, Phys. Rev. B, 49, 14251;

Kresse, G. & Furthmüller, J. 1996, Phys. Rev. B, 54, 11169

Kuhlbrodt, S., Holst, B., & Redmer, R. 2005, Contrib., Plasma Phys., 45, 73

Lenosky, T.J., Bickham, S.R., Kress, J.A., Collins, L.A. 2000, Phys. Rev. B61, 1

Mahaffy, P.R., Niemann, H.B., Alpert, A., Atreya S.K., Demick, J., Donahue, T.M., Harpold, D.N, & Owen, T.C. 2000, J. Geophys. Res.105, 15061

Mattsson, T.R. & Desjarlais M.P. 2006, Phys. Rev. Lett., 97, 017801

Mazevet, S., Kress, J.D., Collins, L.A., & Blottiau, P. 2003, Phys. Rev. B67, 054201

Mermin, N.D. 1965, Phys. Rev., 137, A1441

Nellis, W.J., Ross, M., Mitchell, A.C., van Thiel, M., Young, D.A., Ree, F.H., & Trainor, R.J. 1983, Phys. Rev. A, 27, 608

Nellis, W.J., Weir, S.T., & Mitchell, A.C. 1996, Science, 273, 936

Nettelmann, N., Redmer, R., & Blaschke, D. 2007, Phys. Part. Nucl. Lett., in press

Norman, G.E. & Starostin, A.N. 1968, Templofiz. Vys. Temp. 6, 410

Norman, G.E. & Starostin, A.N. 1970, Templofiz. Vys. Temp. 8, 413

Nosé, S. 1984, J. Chem. Phys., 81, 511

Blöchl, P.E. 1994, Phys. Rev. B50, 17953

Kresse, G. & Joubert, D. 1999, Phys. Rev. B, 59, 1758

Perdew, J.P., Burke, K., & Ernzerhof, M. 1999, Phys. Rev. Lett.., 77, 3865

Peebles, P.J.E. 1964, ApJ, 140, 328

Pfaffenzeller, O., Hohl, D., & Ballone, P. 1995, Phys. Rev. Lett., 74, 2599

Pollack, J.B., Hubickyj, O., Bodenheimer, P., Lissauer, J.J., Podolak, M., & Greenzweig, Y. 1996, Icarus, 124, 62

Sato, B. et al. 2005, ApJ, 633, 465

Saumon, D. & Chabrier, G. 1992, Phys. Rev. A, 46, 2084

Saumon, D., Chabrier, G., & Van Horn, H.M. 1995, ApJS, 99, 713

Saumon, D. & Guillot, T. 2004, ApJ, 609, 1170

SESAME: Los Alamos National Laboratory Equation of State Database 1992, LANL report no. LA-UR-92-3407, Lyon, S.P. & Johnson, J.D. (eds.)

Stevenson, D.J. 1982, Ann. Rev. Earth Planet Sci. 10, 257

Stevenson, D.J., & Salpeter E.E. 1977, ApJS35, 221

Stevenson, D.J., & Salpeter E.E. 1977, ApJS35, 239

van Thiel, M. et al. 1973, Phys. Rev. Lett., 31, 979

Vorberger, J., Tamblyn, I., Militzer, B., & Bonev, S.A. 2006, Phys. Rev. B, 75, 024206

Wagner, W. & Prusz A. 2002, J. Phys. Chem. Rev. Data, 31, 387

Feistel, R. & Wagner, W. 2006, J. Phys. Chem. Rev. Data, 35, 1021

Weir, S.T., Mitchell, A.C. & Nellis, W.J. 1996, Phys. Rev. Lett., 76, 1860

von Zahn, U., Hunten, D.M., & Lehmacher, G. 1998, J. Geophys. Res., 103, 22815

Zeldovich, Ya.B. & Landau, L.D. 1944, Zh. Eksp. Teor. Fiz., 14, 32

Zharkov V.N. & Trubitsyn V.P. 1978, Physics of planetary interiors (AASeries; Tucson/AZ: Parchart)

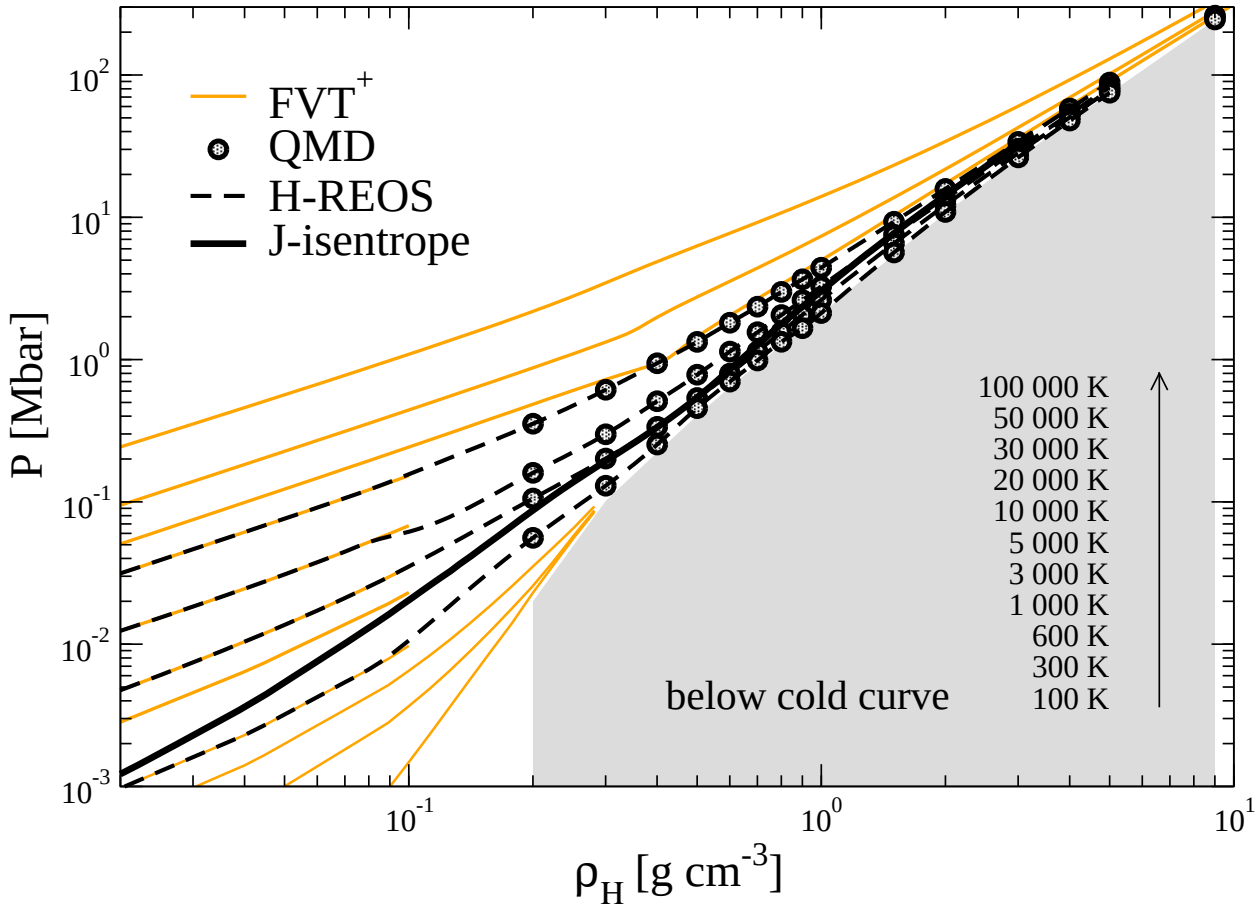

Fig. 1.— (Color online) Isotherms for hydrogen for different EOS tables: FVT$^+$, QMD, and H-REOS. The thick line shows the pressure-density relation of the hydrogen fraction of a typical Jupiter isentrope and the grey area masks the non-accessible region below the cold-curve represented here by a 100 K isotherm of QMD data.

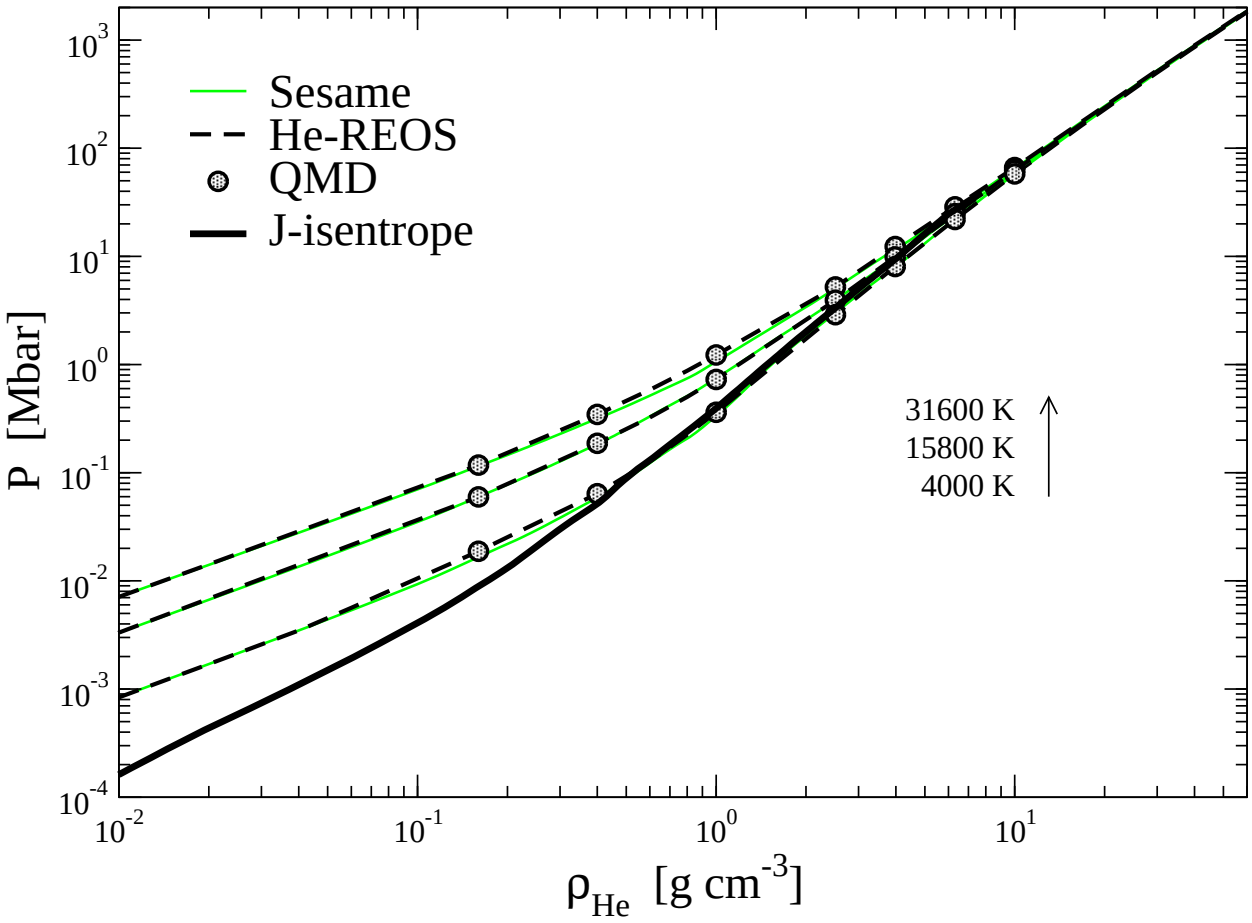

Fig. 2.— (Color online) Isotherms for helium for T=4000, 15800, 31600 K and three different EOS tables: Sesame 5761, QMD data, and He-REOS. The thick line shows the pressure-density relation of the helium fraction along a typical Jupiter isentrope.

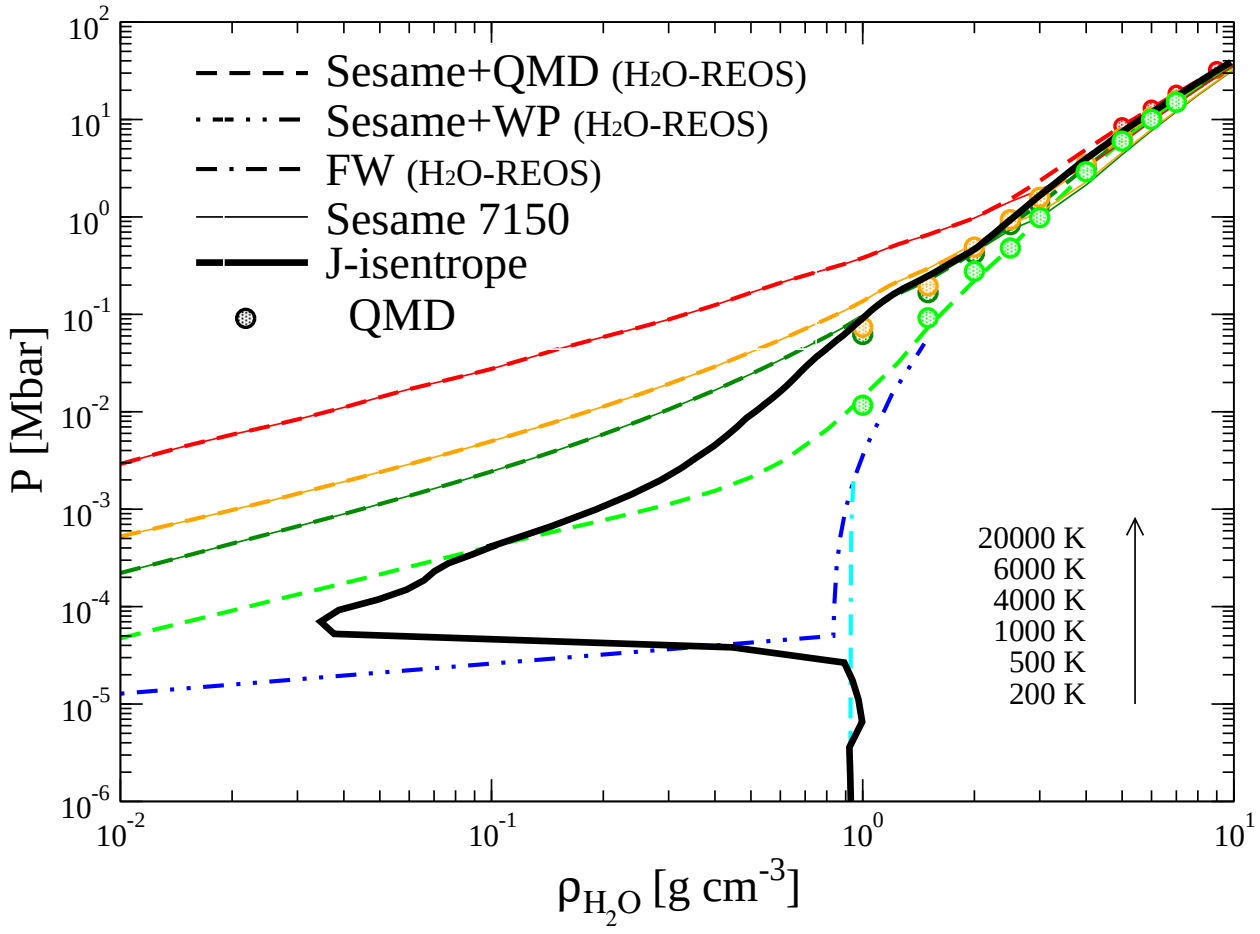

Fig. 3.— (Color online) Isotherms for H_2O for T=200, 500, 1000, 4000, 6000, and 20000 K according to different EOS tables: a combination of QMD and Sesame 7150 for $T \geq 1000$ K, a combination of WP and Sesame 7150 for $T < 1000$ K, FW Feistel & Wagner (2006) for ice I, Sesame 7150, and QMD data. The thick line shows the pressure-density relation of the H_2O fraction along a typical Jupiter isentrope. All these isotherms are incorporated into H_2O-REOS.

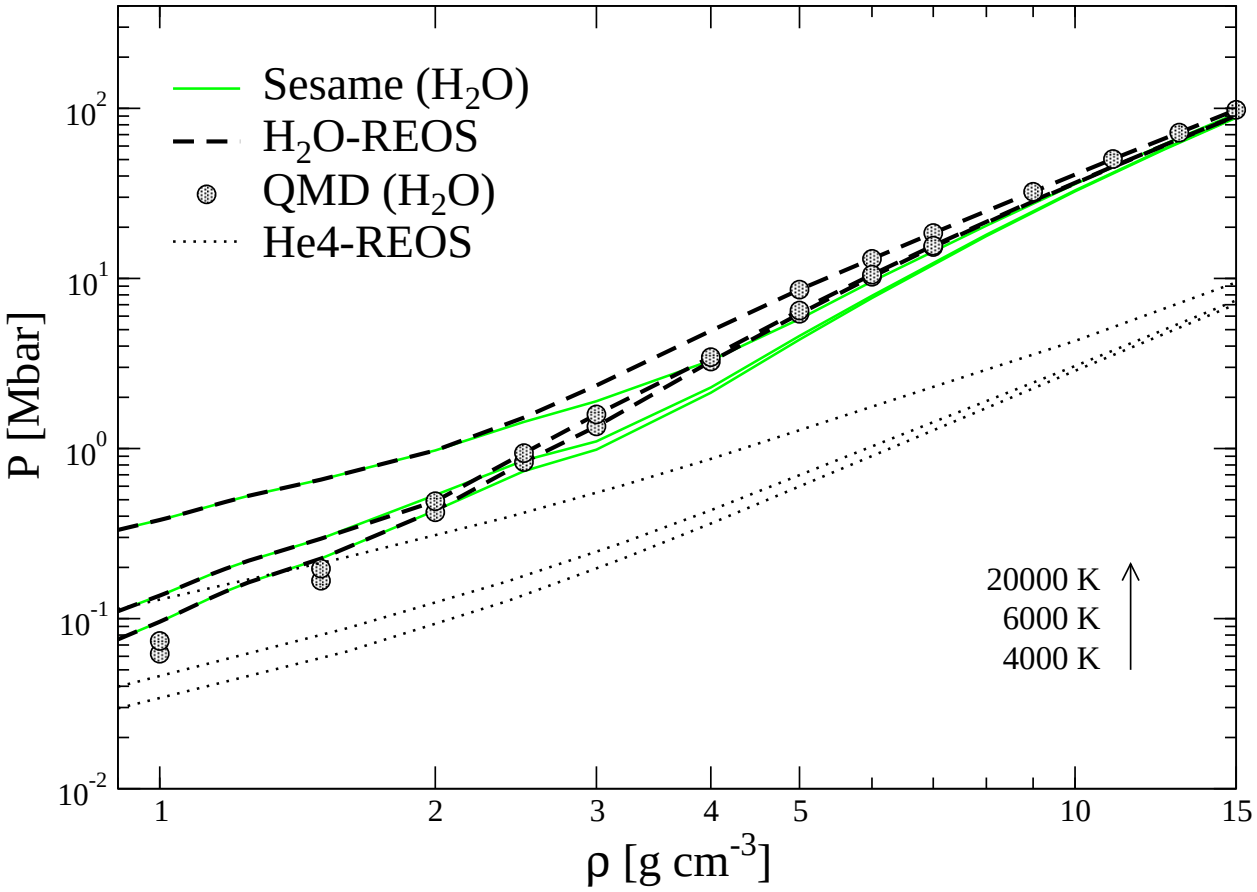

Fig. 4.— (Color online) Isotherms of the Z-component for T=4000, 6000, and 20000 K according to different EOS: Sesame 7150 for H_2O, QMD data for H_2O, H_2O-REOS, and He4-REOS.

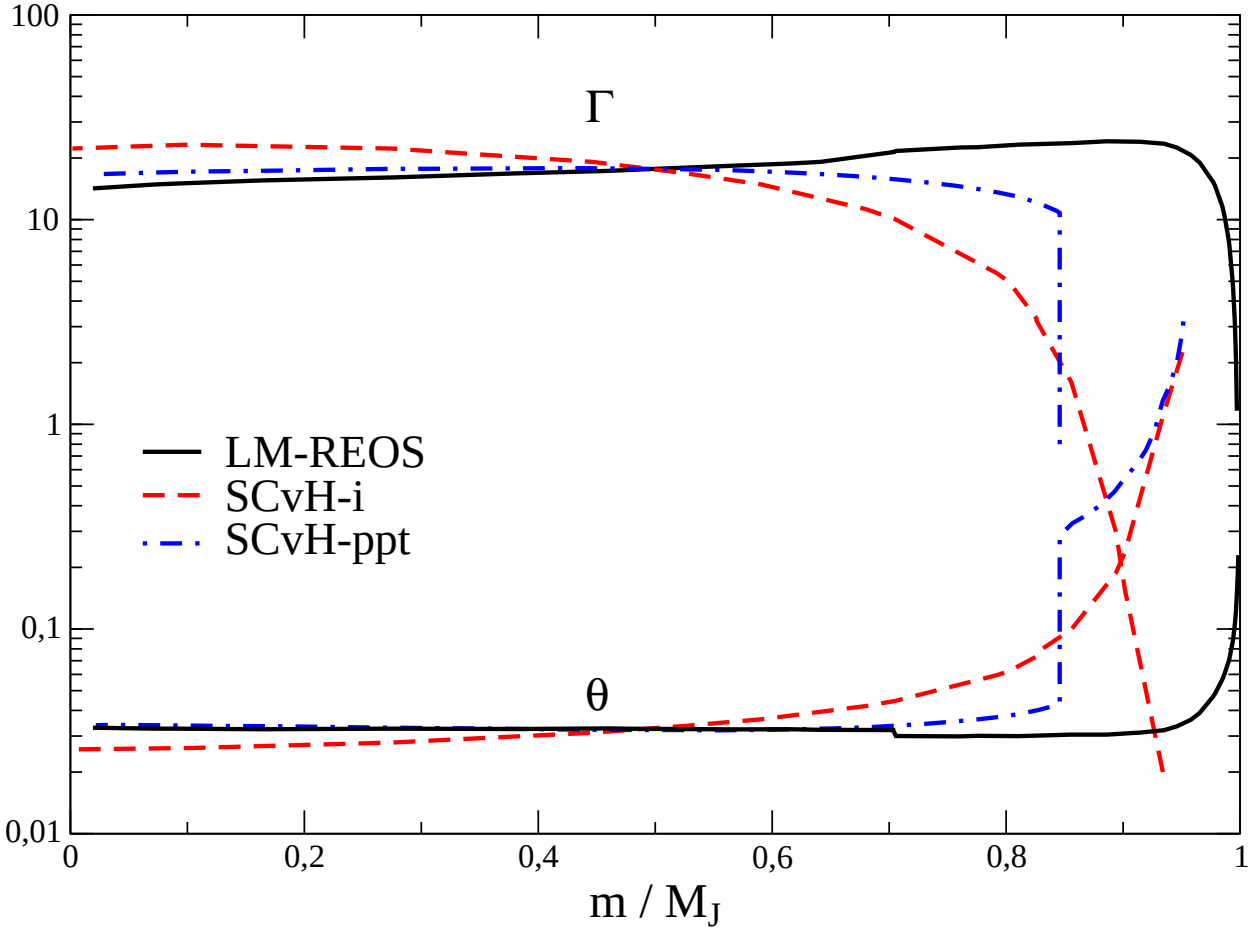

Fig. 5.— (Color online) Coupling parameter Γ and degeneracy parameter Θ inside Jupiter for different EOS: LM-REOS, SCvH-i, and SCvH-ppt.

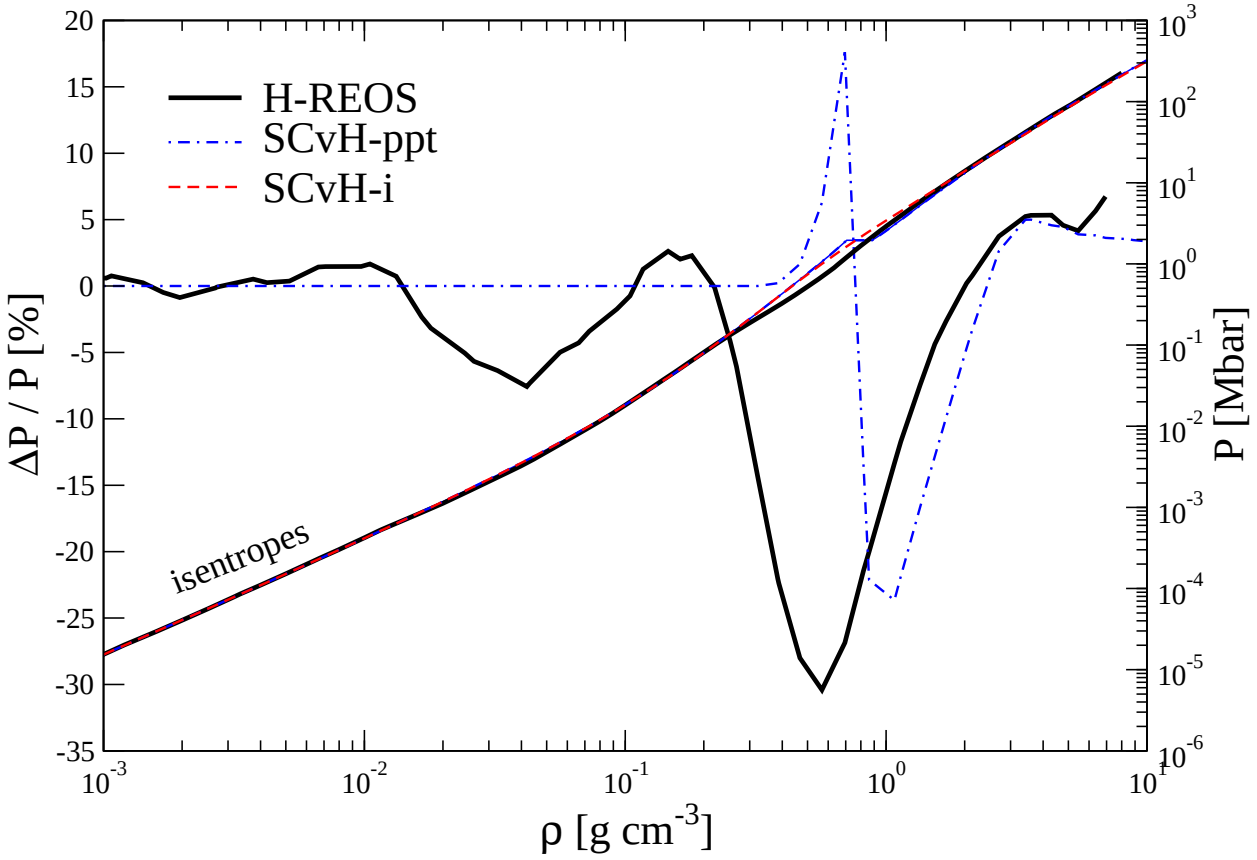

Fig. 6.— (Color online) Hydrogen adiabats for Jupiter, determined by T=165 K at P=1 bar, computed with three different hydrogen EOS: H-REOS, SCvH-i, and SCvH-ppt. The scale on the right shows absolute pressures and the scale on the left shows relative differences in pressure with respect to the SCvH-i-adiabat.

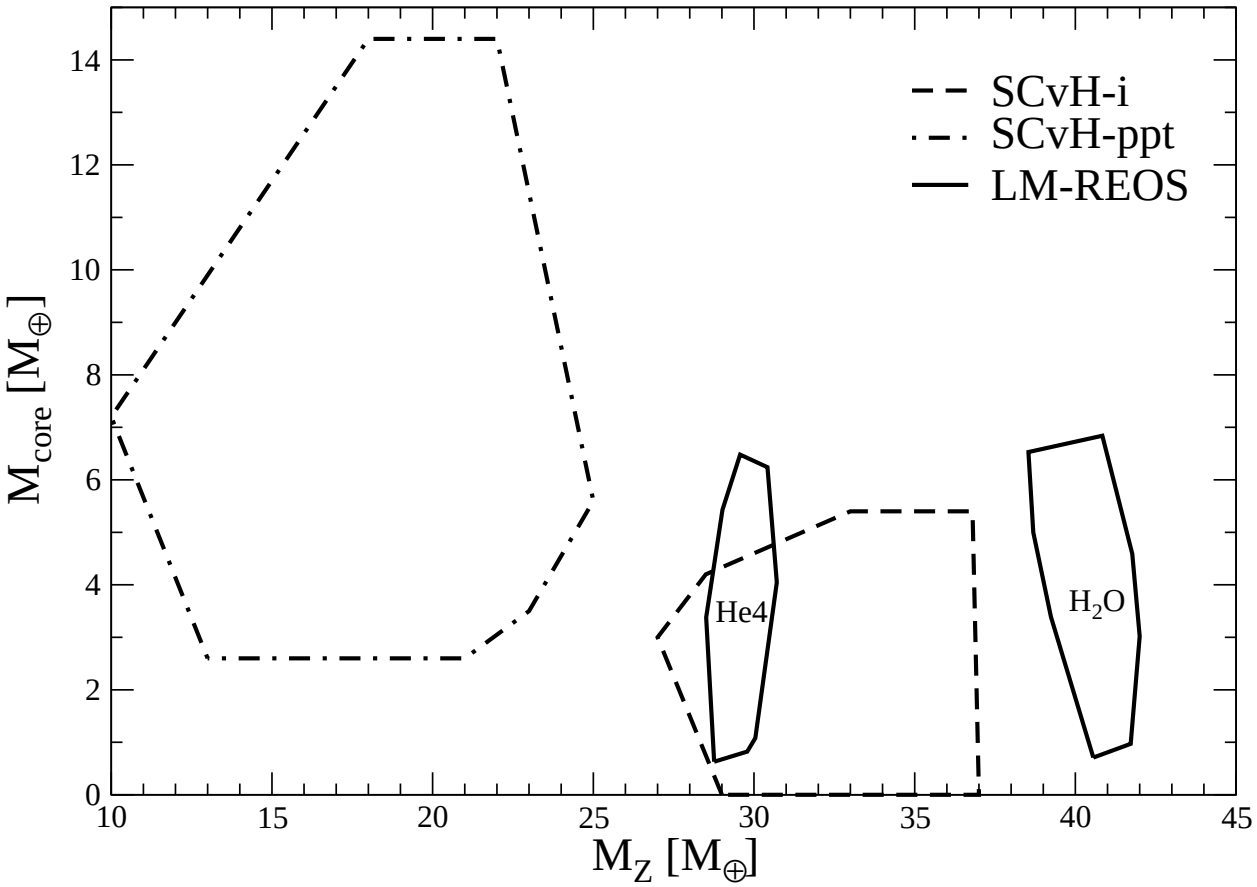

Fig. 7.— Core mass and total mass M_Z of heavy elements in units of Earth masses for three different EOS. Solutions with LM-REOS (solid lines) demonstrate a strong influence of the choice of the EOS of metals to the resulting total heavy element abundance and are displayed in seperate boxes labeled 'He4' and 'H_2O', respectively.

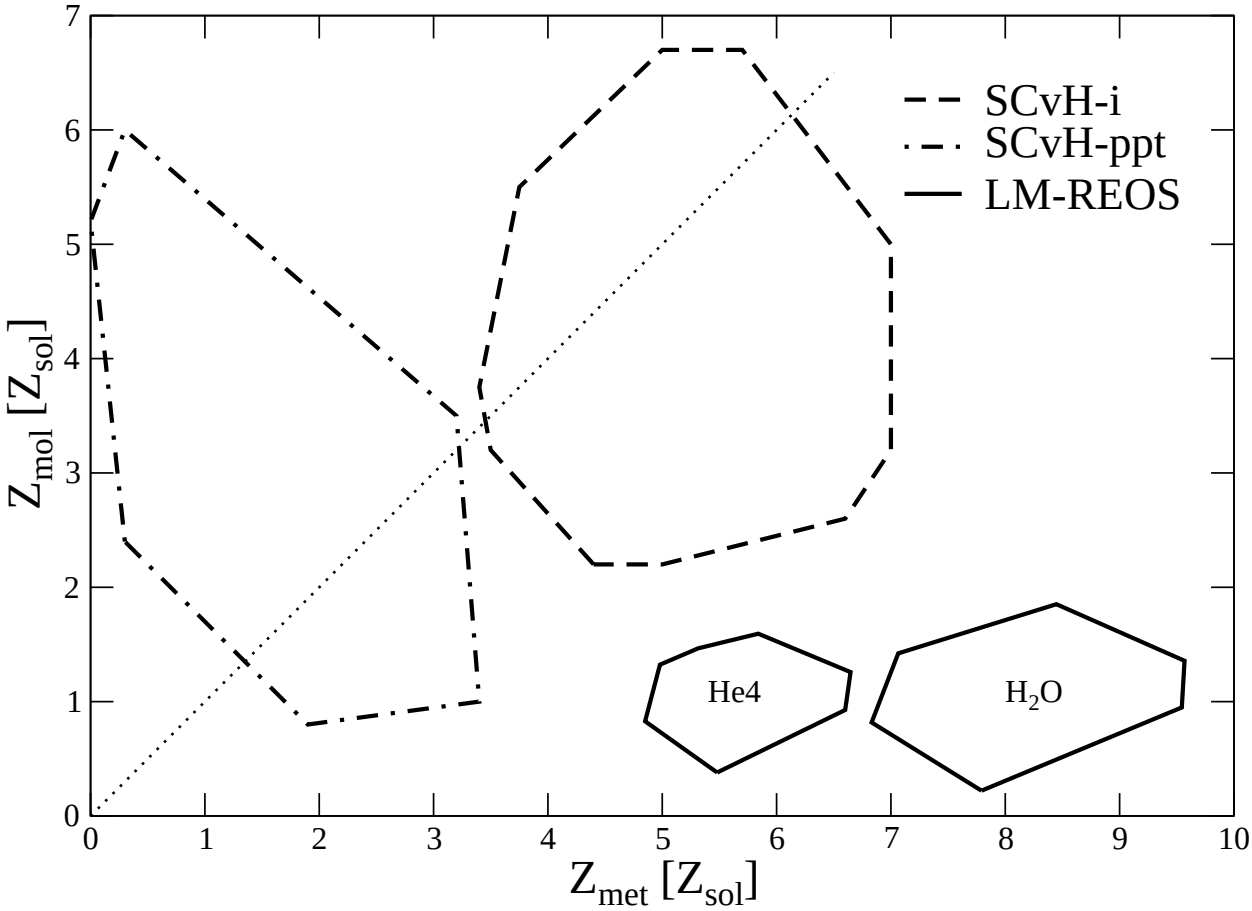

Fig. 8.— Abundance of heavy elements in solar units in the molecular layer ($Z_{\rm mol}$) and in the metallic layer ($Z_{\rm met}$) for three different EOS. The dotted line indicates equal abundances. Solutions with LM-REOS (solid lines) demonstrate a strong influence of the choice of the EOS of metals to the resulting value of $Z_{\rm met}$ and are displayed in seperate boxes labeled 'He4' and 'H_2O', respectively.

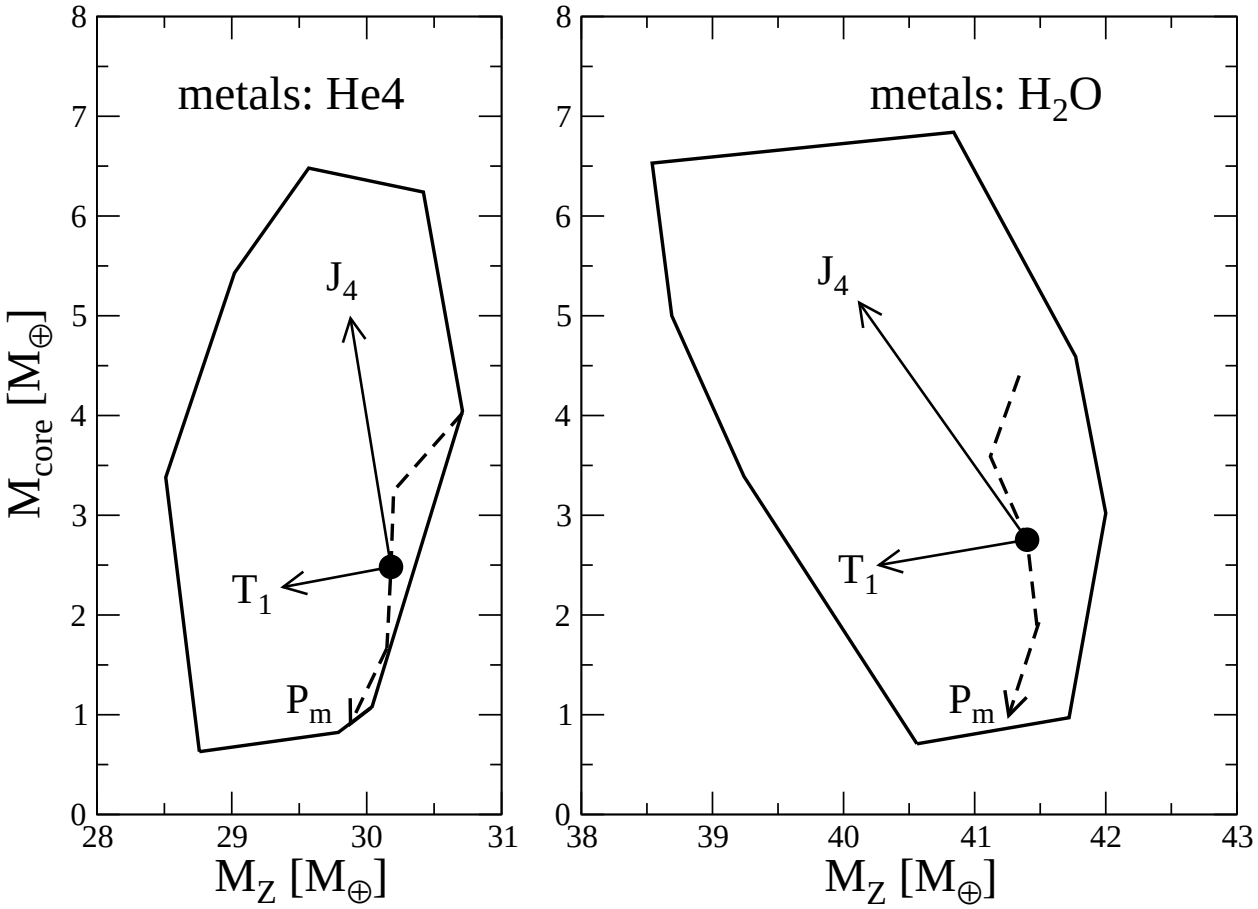

Fig. 9.— Same as Fig. 7 but only for solutions using LM-REOS. The arrows indicate the shifts of the reference solution ($T_1 = 170$ K, $\bar{Y} = 0.275$, $P_{\rm m} = 4$ Mbar, $J_4/10^4 = -5.84$) if T_1 is decreased to 165 K, $|J_4|$ increased by 1 σ, or $P_{\rm m}$ enhanced from 3 to 5 Mbar.

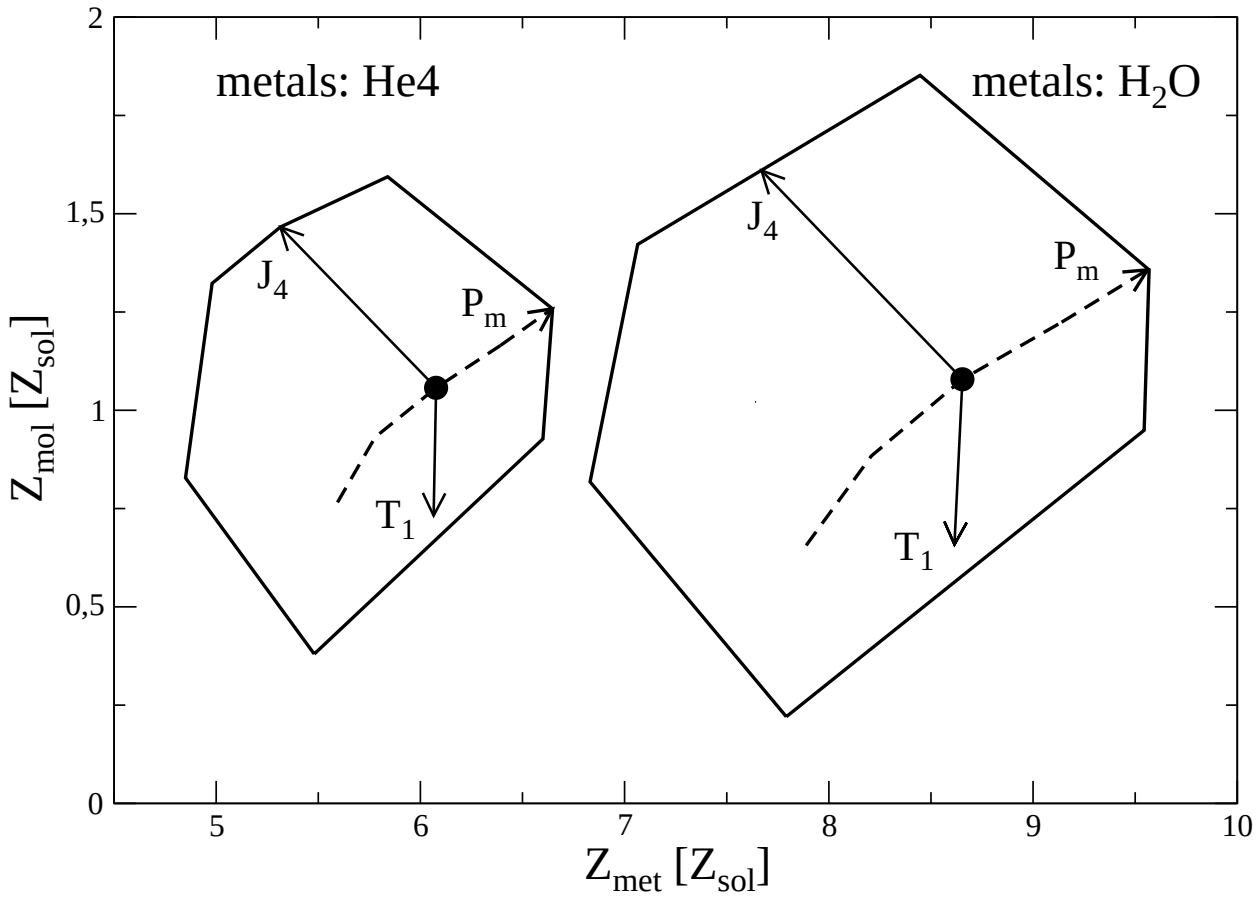

Fig. 10.— Same as Fig. 8 but only for solutions using LM-REOS. See Fig. 9 for a description.

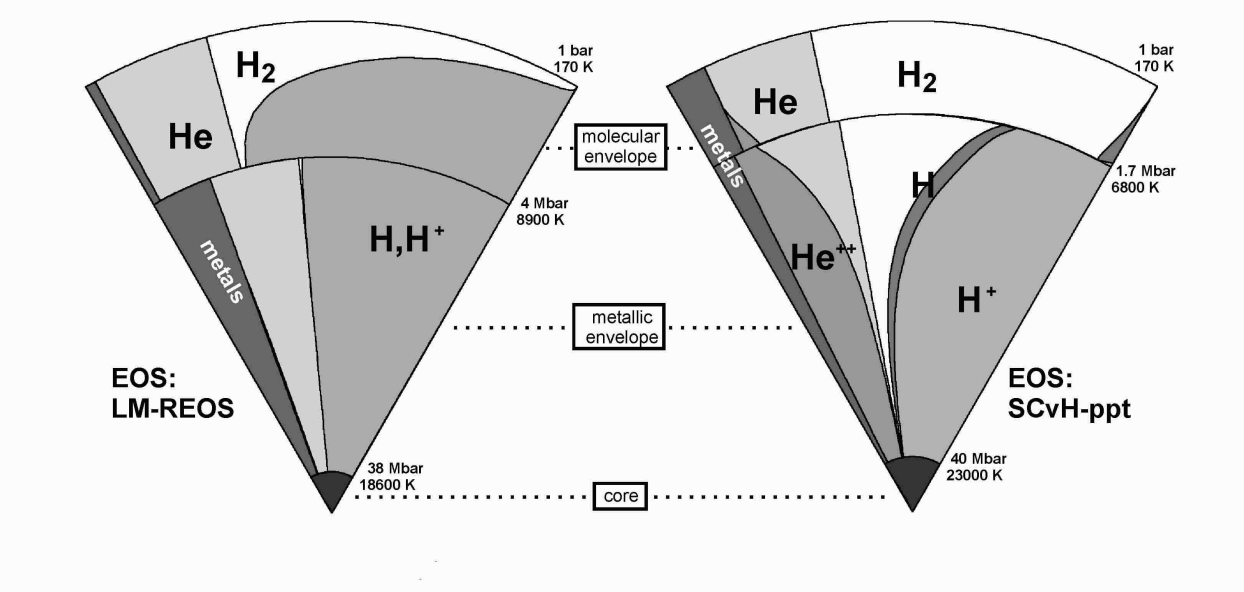

Fig. 11.— Schemes of Jupiter models satisfying the same constraints; left: model J11a, right: model J11b. At the layer boundaries the values of pressure and temperature are given. The abundances of metals and of chemical species along the radius are indicated by grey scales. An arc segment corresponds to 100% in mass. For model J11a, an ASCII data table containing the profiles of pressure, temperature, density, composition and the figure functions along the radius can be found in the electronic edition of this Journal.